

Article

Influence of Masonry Infill Walls on the Seismic Assessment of Non-Seismically Designed RC Framed Structures

Rodrigo Falcão Moreira ^{1,*}, Humberto Varum ² and José Miguel Castro ²¹ CONSTRUCT-LESE, School of Engineering, Polytechnic of Porto, 4249-015 Porto, Portugal² CONSTRUCT-LESE, Faculty of Engineering, University of Porto, 4200-465 Porto, Portugal

* Correspondence: rem@isep.ipp.pt

Abstract: This paper examines how the decision to include (or exclude) masonry infill walls in the modelling of non-seismically designed RC framed structures can affect the results of the EC8-3 seismic assessment process. A frequently used macro-modelling technique for the simulation of infill panels within bounding RC members is first reviewed. A case-study application follows in which the seismic assessment of a sample structure is carried out, with and without considering the effect of its infill walls, using nonlinear static and dynamic analysis models. The obtained results are then discussed according to the applicable limit states' performance requirements, and conclusions are drawn regarding the overall outcome. The study indicates that, when low and medium seismic input motions constitute the base demand for the assessment of older-type RC framed buildings, the protection provided to the RC members by the confined masonry infill panels should not be neglected. Moreover, it shows that the identification of the most likely collapse mechanism might also be significantly influenced by the modelling decision in question. As such, the default recommendation is to include masonry infill walls in the modelling of such structures.

Keywords: RC buildings; seismic assessment; numerical modelling; masonry infills



Citation: Falcão Moreira, R.; Varum, H.; Castro, J.M. Influence of Masonry Infill Walls on the Seismic Assessment of Non-Seismically Designed RC Framed Structures. *Buildings* **2023**, *13*, 1148. <https://doi.org/10.3390/buildings13051148>

Academic Editors: Marco Di Ludovico and Harry Far

Received: 4 February 2023

Revised: 2 April 2023

Accepted: 24 April 2023

Published: 26 April 2023



Copyright: © 2023 by the authors. Licensee MDPI, Basel, Switzerland. This article is an open access article distributed under the terms and conditions of the Creative Commons Attribution (CC BY) license (<https://creativecommons.org/licenses/by/4.0/>).

1. Introduction

Infill panels are commonly used in RC buildings as interior partitions and external walls. Consequently, they are normally treated as non-structural elements and are expected to develop no significant interaction with the main structural system. However, while this hypothesis might stand for static loads, it will not be valid for earthquake loads. In the latter case, infill panels are known to develop strong interactions with the bounding RC members. Through their in-plane horizontal stiffness and strength, infill walls decrease storey drift demands and increase storey lateral force, while significantly contributing to the global energy dissipation capacity. On the other hand, they reduce the structure's global ductility and induce additional shear forces on column members, which can cause them to experience brittle shear failure mechanisms (as frequently observed in past earthquakes). Example capacity curves for bare and infilled frames are shown in Figure 1, where the above-referred increments in stiffness and strength are evident at the initial stage. However, the sudden deterioration of the infill panels' capacity is also clear (demonstrating the referenced global ductility reduction), as well as the consequent drop in the total base shear values to ones close to those of the bare frames.

While several authors (e.g., [1–3]) have demonstrated the beneficial contribution of infill walls to the overall seismic performance of RC buildings—especially when the latter exhibit limited lateral resistance and provided that the seismic demand does not exceed the deformation capacity of the former—others (e.g., [4–6]) have identified situations which may lead to its deterioration. For instance: (i) the interruption of infill walls in height may lead to the formation of soft-storeys; (ii) an irregular in-plan distribution of infill walls may generate torsional structural response to the translational horizontal components of the

seismic action. Consequently, many have argued that the only feasible way to account for the positive and negative effects of infill walls is to directly include them in the analytical models used for seismic design and assessment purposes.

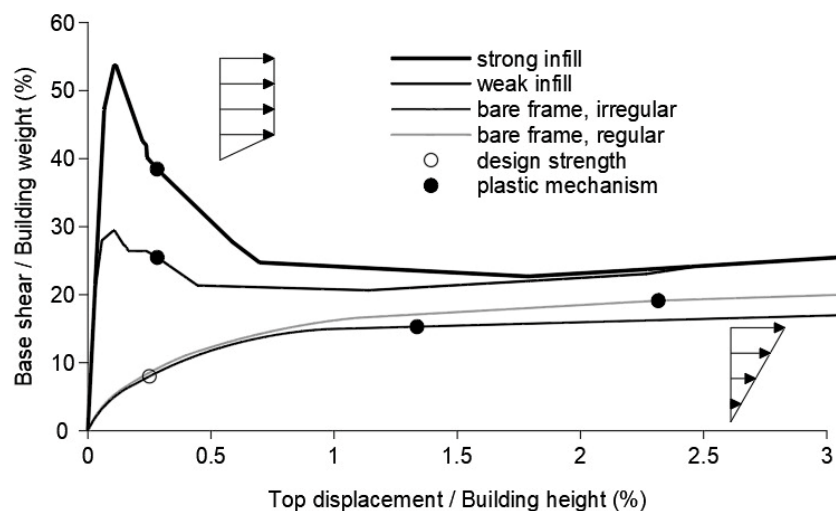


Figure 1. Force-displacement curves for bare and infilled frames (adapted from [7]).

This paper thus examines how the decision to include (or exclude) masonry infill walls in the modelling of non-seismically designed RC framed structures can affect the results of the EC8-3 [8] seismic assessment process. In that cause, a case study application is presented in which the seismic assessment of a sample structure is carried out, with and without considering the effect of its infill walls, using nonlinear static and dynamic analysis models. The obtained results are then discussed according to the applicable limit states' performance requirements, and conclusions are drawn regarding the overall outcome. The obtained results are in line with the experimental results of the ICONS research programme [9], which also contributed to the validation of the developed calculation models. That validation was performed by Falcão Moreira [10] but intentionally left out of this paper, as it would make it even longer. However, the readers are referred to the discussions included in that work. Overall, this paper highlights the importance of considering masonry infill walls in the seismic assessment of older-type RC structures and emphasizes the need for accurate modelling and analysis to obtain reliable seismic performance results.

2. Numerical Macro-Modelling of Masonry Infill Walls

Several attempts have been made to realistically describe the behaviour of infill walls, including the potential failure modes as observed in experimental tests (i.e., shear cracking; compression failure; and flexural cracking). Different modelling techniques have thus been proposed, which can be divided into two main categories in terms of simulation approach: (i) fundamental or micro-models, and (ii) simplified or macro-models [11]. The plane finite elements and the equivalent truss models are typical examples of the first and second categories, respectively. Micro-models can simulate structural behaviour in detail (e.g., large displacements; rotation and sliding between blocks; automatic detection of new contacts during calculations), provided that adequate constitutive models are used. However, they are computationally intensive and difficult to apply to the analysis of large structures due to the amount of information that is required. On the other hand, macro-models exhibit obvious advantages in terms of computational simplicity and efficiency. Their formulation is based on a physically reasonable representation of the behaviour of the infilled frame. They can describe the overall response, but often do not capture local phenomena appearing between the infill panels and the surrounding RC frame. However, they represent a good compromise between accurate representation and numerical efficiency [12].

A detailed review of the existing proposals for modelling the seismic response of infilled frames is beyond the scope of this work. Readers are referred to the works of Crisafulli et al. [13] and Dias-Oliveira et al. [14] for a thorough review of the most relevant publications on this matter, as well as to the following (more specific) works: Kakaletsis and Karayannis [15] and Messaoudi et al. [16] on the influence of openings on infill walls; Sassun et al. [17] on the in-plane behaviour of infill walls; and Furtado et al. [18], on the out-of-plane behaviour of infill walls. However, due to the relevance of this matter for the performance-based seismic assessment of existing RC buildings, the following sections summarize a modelling approach that can be adopted within most software platforms. The described model is capable of accounting for the local effects in the surrounding frame due to the presence of the infill panel without a significant increase in the complexity of the analysis. Further details on the implementation of this modelling approach can be found in [11,12].

2.1. Equivalent Strut Approach

The equivalent strut approach represents the strut action of the infill wall through the introduction of diagonal compression-only struts. Crisafulli et al. [13] studied the influence of the three strut models shown in Figure 2 on the structural response of infilled frames, focusing on the stiffness of the structure and the actions induced in the surrounding frame. The obtained results were compared to those of a more refined finite element model of the case study structure. The effects on the bending moment and shear force induced in the columns were then examined in detail to provide insight into which approach provided the most accurate representation of the frame-infill interaction.

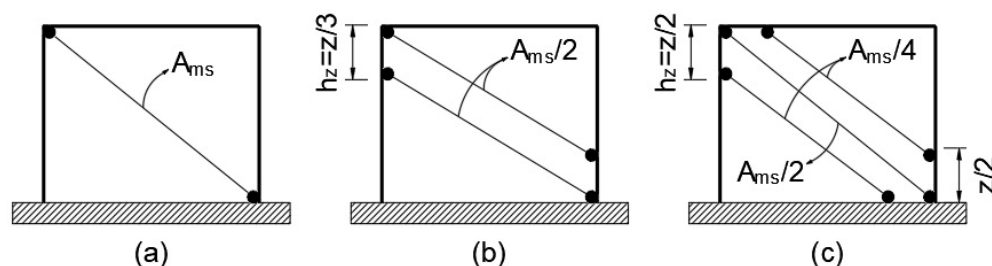


Figure 2. Possible strut models: (a) single-strut; (b) double-strut; (c) triple-strut [19].

The three models behaved similarly in terms of lateral stiffness, leading to the conclusion that (as confirmed by Celarec and Dolšek [20] and others) the single-strut model constitutes a good enough tool for the prediction of the overall response of the infilled frame, offering adequate estimations of lateral stiffness and axial forces induced in frame members. However, regarding the bending moments and shear forces induced in the surrounding frame, these were underestimated by the single-strut model. On the other hand, the double- and triple-strut models provided accurate enough estimates on these parameters, with the double-strut model having the advantage of being less complex to implement. The latter was adopted by Crisafulli [19] within his proposal of an advanced nonlinear cyclic model for masonry panels, offering the possibility of modelling the material with different levels of accuracy according to the amount of available information. A summary of this proposal is presented in the next subsection.

Strut models have been adopted during the last twenty-five years in studies analysing the influence of masonry infills on the seismic response of RC frames. For instance, Dolšek and Fajfar [21] applied the single-strut modelling approach, while Celarec and Dolšek [20] used the double-strut model and Jeon et al. [22] used the triple-strut model. However, no consensus has been reached as to which approach is the most realistic, since it depends on what the analyst requires and whether the layout of elements accurately represents the actual conditions of the infills [12]. While it may seem that the triple-strut modelling approach represents the best option to capture the complete behaviour of the infills, Celarec

and Dolšek [20] believe that a double-strut approach will suffice, since the actual connectivity and contact between the top of an infill wall and the underside of the upper beam is typically quite weak. Moreover, the forces induced on the surrounding beam elements need not be modelled with such precision, since most of the problems that have been observed in past earthquakes are related to the interaction of infill walls with column members.

2.2. Element Formulation

The nonlinear cyclic model for masonry panels developed by Crisafulli [19], featuring a double-strut modelling approach, can provide good insight on the frame-infill interaction effects at reasonable modelling and computational costs [11]. As illustrated in Figure 3, the proposed nonlinear element is defined by two components: (i) compression/tension struts; (ii) and shear springs. Each panel is thus represented by four axial struts and two shear springs; each diagonal direction features two parallel struts to account for axial forces and deformation across two opposite corners, and one shear spring to account for bed-joint resistance and sliding forces. As the shear spring acts solely across the diagonal that is under compression, its “activation” depends on the deformation of the panel. Moreover, four internal nodes are employed to account for the actual points of contact between the frame and the infill panel (i.e., to account for the width and height of the columns and beams, respectively), whilst four dummy nodes are introduced to account for the contact length between the frame and the infill panel.

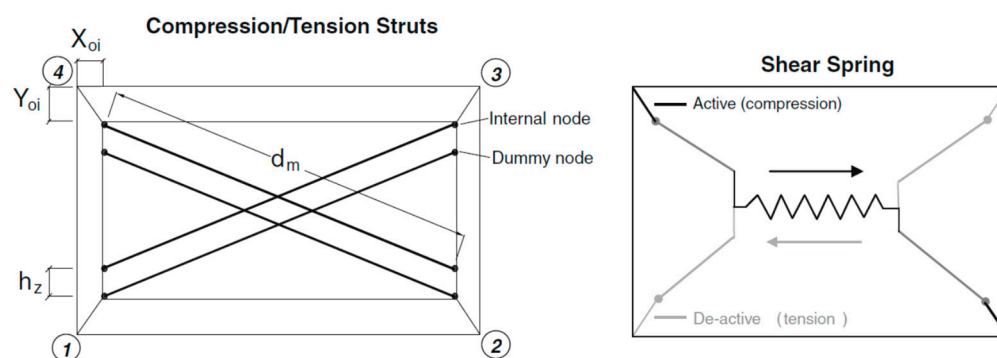


Figure 3. Infill panel model [23].

The total stiffness of the element is distributed proportionally between the shear spring (K_S) and the struts (K_A) according to Equations (1) and (2), where γ_s is the percentage of the total stiffness assigned to the shear spring; E_m is the masonry’s elastic modulus; A_{ms} is the area of the struts; and d_m and θ are the length and the inclination, respectively, of the diagonal of the infill panel. The stiffness matrix and coordinates transformation procedure are obtained from the equilibrium and compatibility of forces and displacements, respectively. All of the internal forces must be transformed to the exterior four nodes where the infill panel element is connected to the frame. Forces and displacements obtained in the dummy nodes must first be transferred to the adjacent internal nodes and then to the external nodes. The transformation of the forces and displacements obtained with the shear spring is simpler because only the step from the internal to the external nodes needs to be carried out. For further numerical details on these procedures, readers are referred to [23]. Readers are also reminded that this model is not capable of modelling potential plastic hinges that develop in the columns, even though the effect of the strut’s eccentricity is considered. If it is important to model the development of plastic hinges in the length of the columns, a different strut configuration must be implemented.

$$K_S = \gamma_s \cdot \frac{A_{ms} \cdot E_m}{d_m} \cdot (\cos \theta)^2 \quad (1)$$

$$K_A = (1 - \gamma_s) \cdot \frac{A_{ms} \cdot E_m}{2 \cdot d_m} \quad (2)$$

Besides the four corner nodes, the following model-calibrating parameters need to be defined to fully characterize the proposed nonlinear element [11]:

- Hysteretic relationship for the compression/tension struts;
- Hysteretic relationship for the shear spring;
- Infill panel thickness (t), which may be simply considered equal to the thickness of the bricks;
- Strut area 1 (A_1), defined as the product of the panel's thickness by the equivalent width of the strut (b_w), normally varying between 10 and 40% of the diagonal of the infill panel (d_m) as concluded by several authors based on experimental data (e.g., [13]);
- Strut area 2 (A_2), taken as a percentage of A_1 and which tries to account for the fact that, due to cracking of the infill panel, the contact length between the frame and the infill decreases as the lateral and (consequently) axial displacement increase, thus affecting the area of the equivalent strut (see [19]);
- Equivalent contact length (h_z), taken as a percentage of the panel's height, effectively yielding the distance between the internal and dummy nodes, so as to consider the contact length z between the frame and the infill panel, as defined by Stafford Smith [24]—for suggestions of values, refer to (e.g., [13]);
- Horizontal and vertical offsets (X_{oi} and Y_{oi}), taken as a percentage of the horizontal and vertical dimensions of the panel, representing the reduction of the latter due to the depth of the frame members (in practical terms, these parameters provide the distance between the external corner and the internal nodes);
- Proportion of stiffness assigned to shear (γ_s), representing the proportion of the panel stiffness that should be assigned to the shear spring (values ranging between 0.50 and 0.75 are suggested in [13]).

The hysteretic relationships (for compression/tension struts and shear springs) that must be supplied to the panel model are briefly discussed in the following subsection. The approach of Crisafulli et al. [13] is referenced, as is that of Decanini et al. [25–27] in conjunction with the modifications proposed by Sassun et al. [17].

2.3. Hysteretic Relationships

The compression/tension cyclic relationship proposed by Crisafulli [19] is based on results that were previously published by other authors. It features the effects of small inner cycles, tension softening and tension stiffening, besides the compression envelope and associated loading, unloading, and reloading rules [11]. Figure 4 illustrates the proposed model. The definition of six mechanical parameters is required to characterize the model: (i) the initial Young modulus E_m ; (ii) compressive strength $f_{m\theta}$; (iii) tensile strength f_t ; (iv) strain at maximum stress ε_m ; (v) ultimate strain ε_{ult} ; and (vi) closing strain ε_{cl} . Comments and recommendations concerning value ranges can be found in [11,19]. Additionally, nine empirical factors, exclusively associated with the cyclic rules, need to be defined within the model. These empirical parameters come as a natural consequence of the infill panels' complex behaviour (explanations about their meaning and recommended value ranges are given in [19]). However, a sensitivity study carried out by Smyrou [28] indicates that only three parameters play relevant roles in the energy dissipation capacity of the infill panel (i.e., the remaining parameters are not expected to have a major impact if changed from the proposed default values).

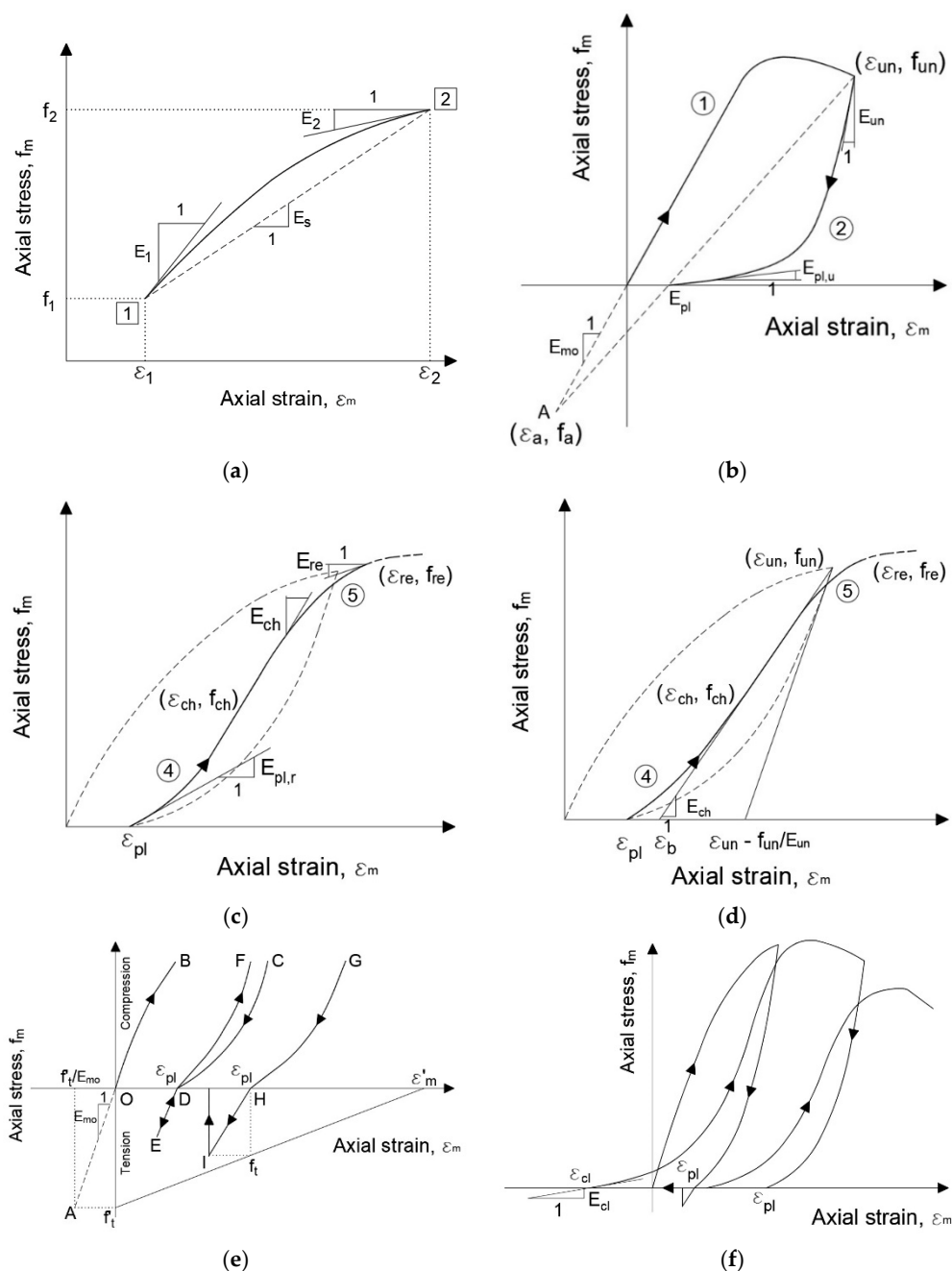


Figure 4. Compression/tension cyclic relationship: (a) unloading and reloading; (b) stress-strain curves for unloading; (c) parameters associated with reloading; (d) definition of the change point for reloading; (e) rule for tensile behaviour; (f) masonry strut hysteretic response (adapted from [19]).

Concerning the cyclic shear relationship, Crisafulli [19] proposed that shear strength is calculated regardless of the failure mechanism (whether it is shear friction failure, diagonal tension failure, or compression failure) taking place in the infill panel. This is a pragmatic approach, combining two shear resistance mechanisms (bond strength and friction resistance between the mortar joints and the bricks), which in practical terms means that shear strength can be expressed as the sum of the initial shear bond strength τ_0 with the product of the friction coefficient μ by the absolute value of the normal compressive force in the direction perpendicular to the bed joints. However, to fully characterize the response curve depicted in Figure 5, two more parameters need to be defined: maximum shear strength τ_{max} and reduction shear factor α_s . Explanations and recommendations about these four parameters can be found in [19]. It should be noted, however, that the actual hysteretic re-

sponse may differ from the one shown in Figure 5, in which the normal stress is assumed to remain constant, since in reality the latter undergoes changes as the infill panel deforms in shear [11]. An alternative implementation of the infill's hysteresis can be found in [12]. The backbone curve is computed using the approach of Decanini et al. [25–27] in conjunction with the modifications proposed by Sassun et al. [17]. This offers the advantage of being a simple model that considers different failure mechanisms, in addition to defining storey drift values (at each limit state) according to experimentally measured values provided by numerous test specimens. However, the existence of openings such as doors or windows was not considered, and neither was the out-of-plane failure of the infill panels. The various terms of the backbone curve are illustrated in Figure 6. For a further description of this implementation, readers are referred to [12].

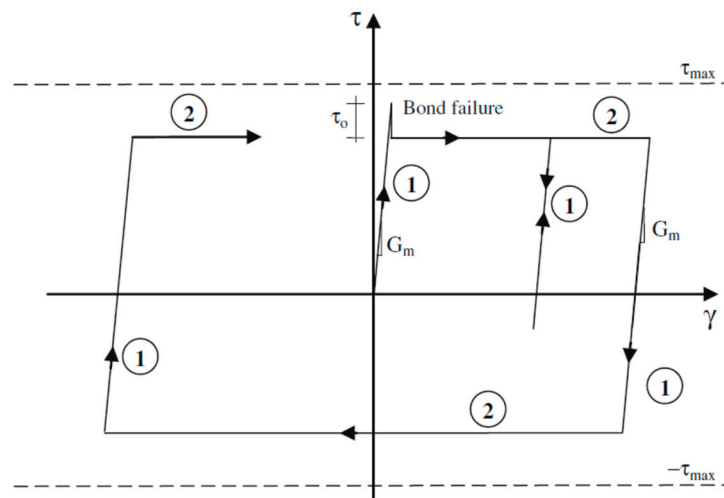


Figure 5. Shear cyclic relationship [19].

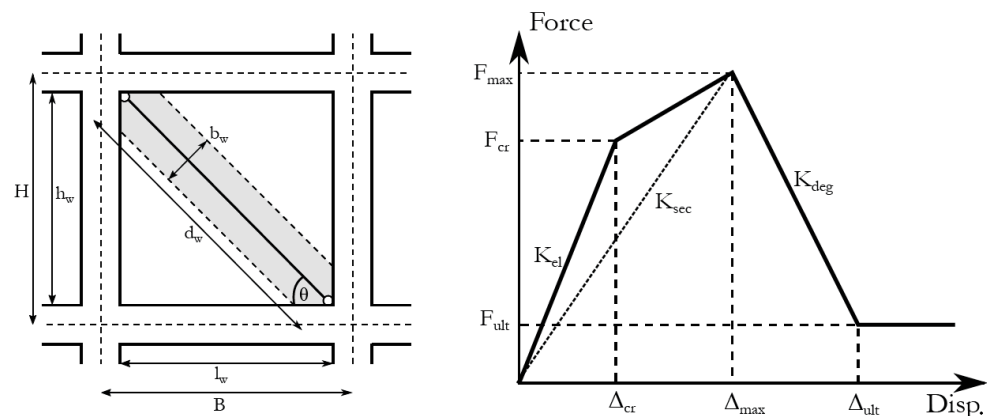


Figure 6. Illustration of the infill's backbone definition [12].

2.4. Modelling of Openings

The presence of openings in masonry panels constitutes an important uncertainty in the evaluation of the behaviour of infilled frames, and, since the 1950s, significant work has been devoted to the investigation of the influence that different configurations (in terms of size and location) might have on strength and stiffness [11]. Unfortunately, though understandably, the large number of involved variables and uncertainties has not yet allowed for an agreement to be reached on this topic and, consequently, has led to various conclusions and recommendations. Engineering judgement and experience, coupled with a thorough consult of the most recent applicable literature, must therefore be used to decide as to how to consider the presence of openings on the panels of the infilled structure under analysis.

As a recommendation, Smyrou et al. [11] suggest reducing the above referred value of the strut area A_1 (hence, the panel's stiffness) in proportion to the area of the opening in relation to that of the panel. As shown in [28], good response predictions might be obtained by reducing the value of A_1 by 30 to 50% if the area of the opening does not exceed 15 to 30% of that of the panel. Concerning the strength of the infill panel, Smyrou et al. [11] suggest that, in the absence of good evidence, no change in its value should be introduced for opening areas up until 30% of the area of the infill panel.

3. Application to a Seismic Assessment Case-Study

3.1. Structural Characterization

The RC structure that was selected is a typical example of the customary design and construction methods used in southern European countries such as Italy, Portugal, and Greece until the end of the 1970s. It was primarily intended to withstand vertical loads, and the reinforcement specifications were based on the construction practices and codes available at that time. Consequently, no specific seismic detailing was enforced, nor were any preferred inelastic dissipation mechanisms assumed, and no specific provisions were made for ductility or strength [29]. Figures 7 and 8 show two elevation views of the structure: one as a bare frame, and another as a frame with brick infilled walls, respectively. Two corresponding full-scale models were built at the ELSA reaction-wall laboratory (Joint Research Centre, Ispra, Italy), within the framework of the ICONS research programme [9]. Pseudo-dynamic (PsD) testing procedures were then used to obtain the experimental seismic response for increasing intensities of the earthquake input motion. The seismic vulnerability of the structure was thus experimentally evaluated, as well as the influence of the infill walls on the global structural response.

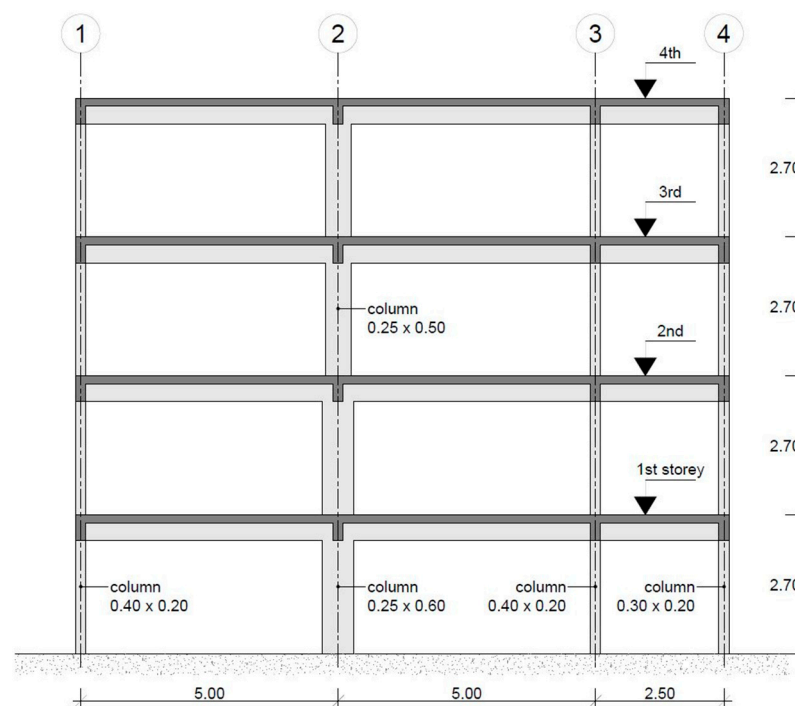


Figure 7. Elevation view of the RC frame (adapted from [29]).

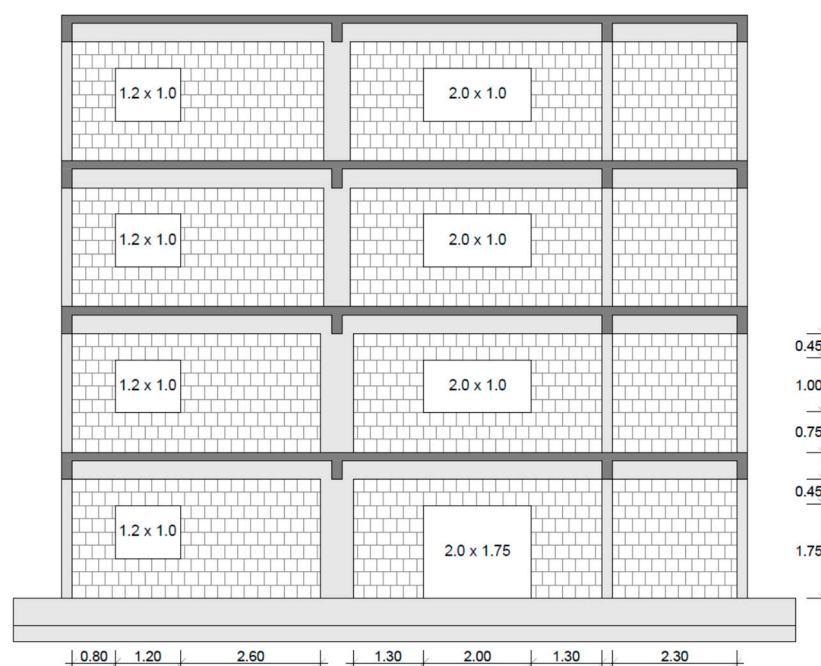


Figure 8. Location and dimensions of the openings on the infill panels (adapted from [29]).

The structure can be described as a four-story frame consisting of three bays, with two spans of 5.0 m and one of 2.5 m, and an inter-story height of 2.7 m. Uniform beams with dimensions of (width) 250 mm \times (height) 500 mm are present on all floors, with equal geometry and reinforcement. Except for the wider interior column (Column 2), all columns have identical geometric properties throughout the structure's height. Column 2 is referred to as a "strong column" due to its ability to mobilize its stronger flexural inertia axis, thus significantly impacting the frame's seismic response. The dimensions of the "strong column" are (width) 250 mm \times (height) 600 mm on the first and second floors, and (width) 250 mm \times (height) 500 mm on the third and fourth floors. Column 1 and Column 3 have dimensions of (width) 400 mm \times (height) 200 mm, while Column 4 has dimensions of (width) 300 mm \times (height) 200 mm. The reinforcement details of beams and columns are shown in Figures 9 and 10, respectively. Regarding the infill walls, the extended external bay features a window opening (1.2 m \times 1.0 m) at every level. The middle bay includes a doorway (2.0 m \times 1.75 m) on the ground floor, and windows (2.0 m \times 1.0 m) on each upper level. The shorter external bay is composed of solid infill panels that lack any openings. Horizontally perforated hollow blocks were used with a unit weight of 42.2 N and the following dimensions: (thickness) 0.120 m \times (base-length) 0.245 m \times (height) 0.245 m. The block units were bedded on the 0.120 m \times 0.245 m face (i.e., with the hollows in the horizontal direction), the mortar joints were approximately 15 mm thick, and a plaster coat of the same thickness was applied on both sides of the walls. The resulting specific weight, by square meter of wall, was 1.45 kN/m². Further details concerning the structure, its material properties, and vertical loading can be found in [9,10,29].

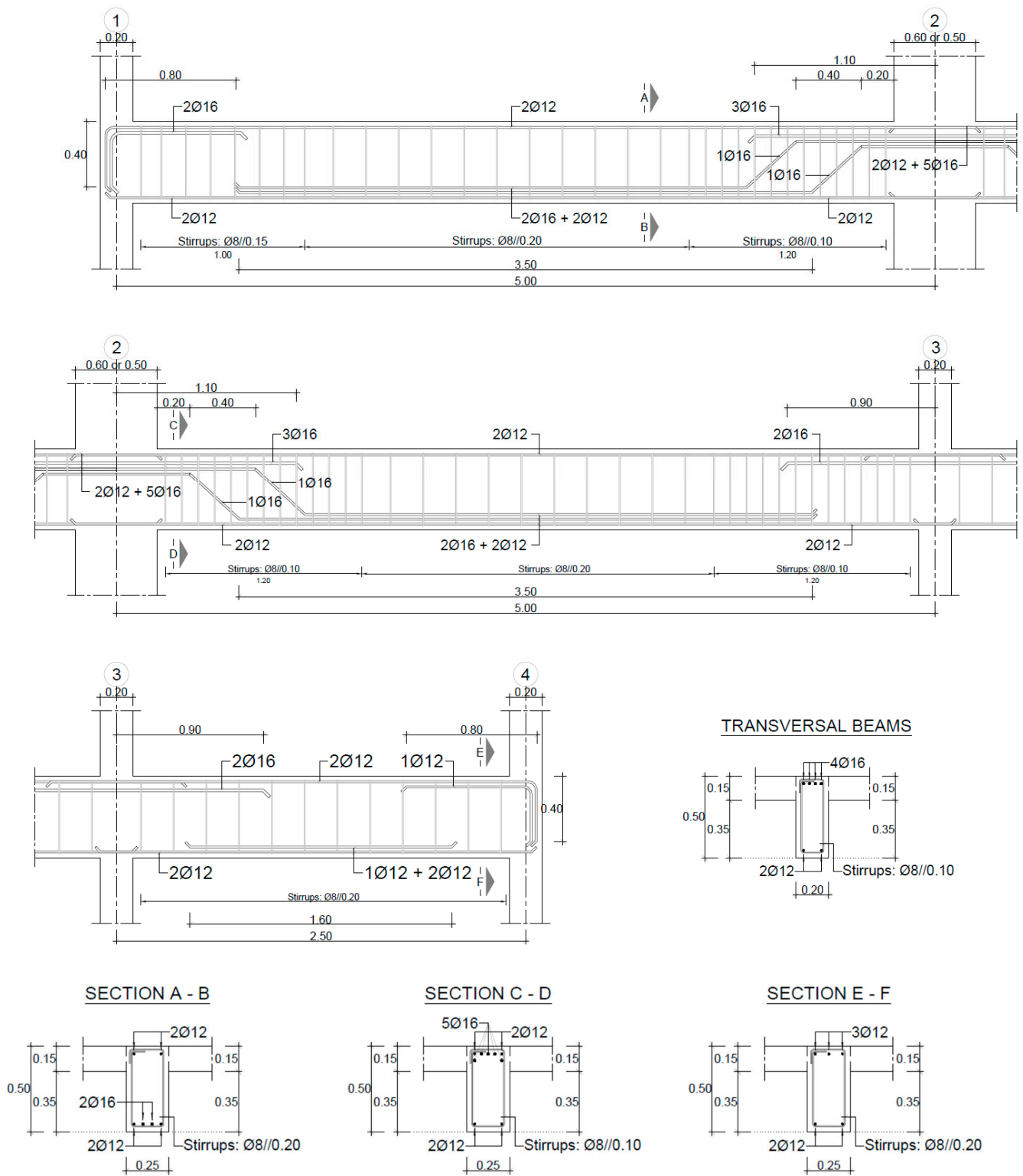


Figure 9. Beam cross-section and reinforcement details (adapted from [29]).

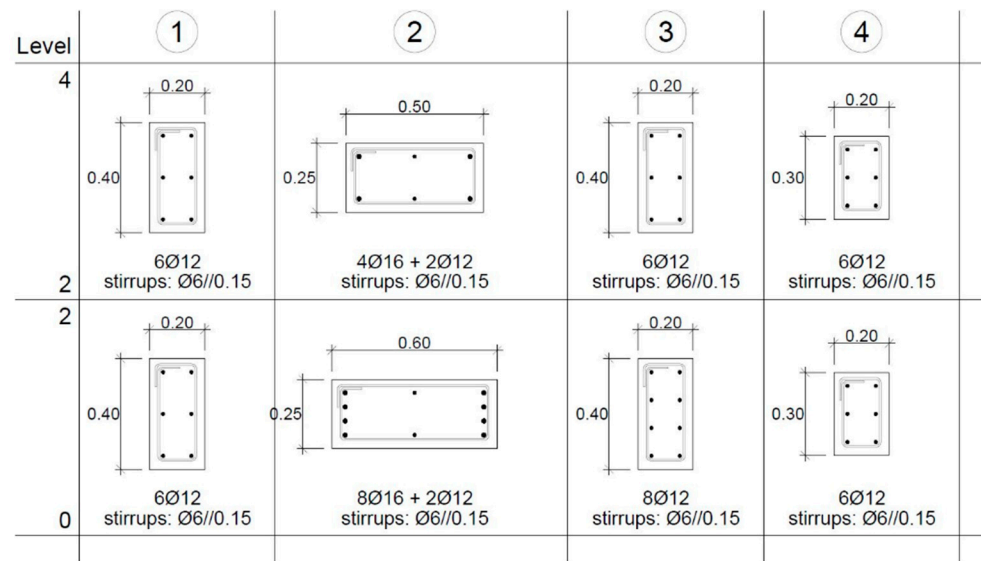
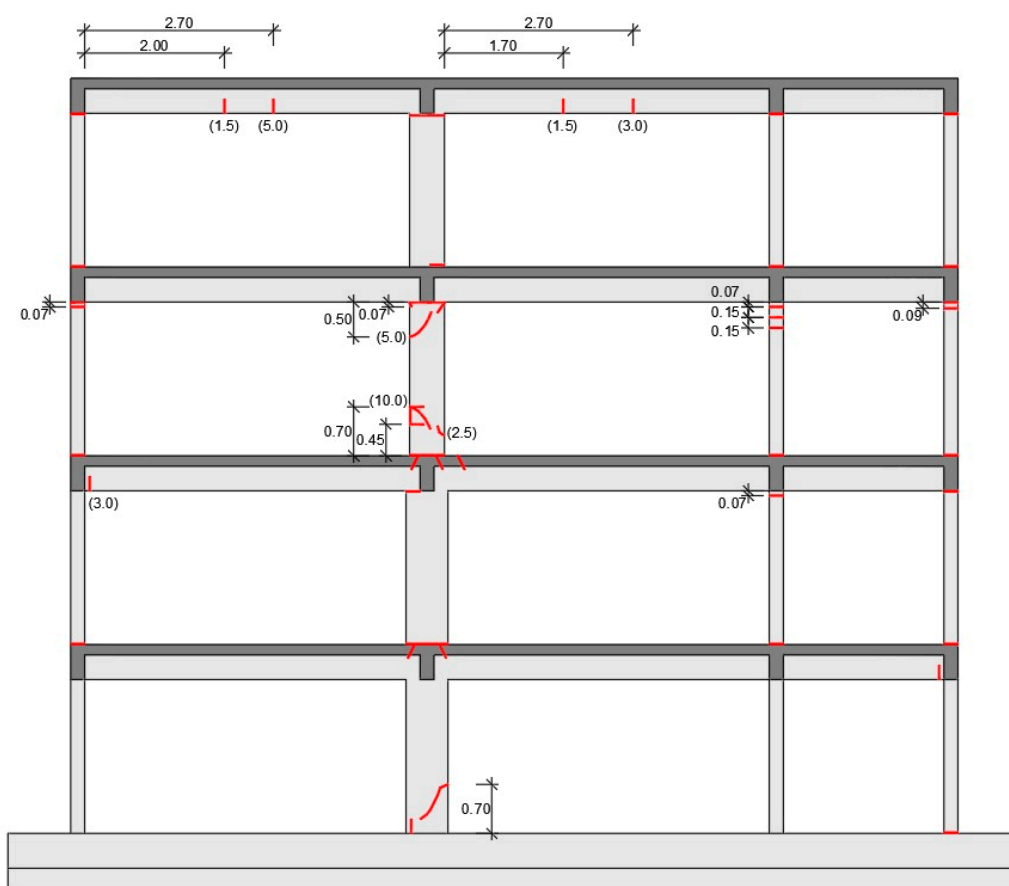


Figure 10. Column cross-section and reinforcement details (adapted from [29]).

3.2. Experimental Results

The above-referenced PsD tests provided results for the bare and infilled frames in terms of modal frequencies, storey displacements, drifts, shear, and damage (the full set of results can be found in [9,10,29]). The input seismic motions were defined so as to be representative of a moderate-high European seismic hazard scenario. The hazard consistent time-series of acceleration (15 s duration) was artificially generated, yielding a set of twelve uniform hazard response spectra for increasing return periods (yrp). Input signals corresponding to the 475-, 975-, and 2000-yrp were then used in the PsD tests (associated PGA values of 0.22 g, 0.29 g, and 0.38 g, respectively). For the purpose of modal identification (before and after each test series), a very low intensity earthquake was applied, allowing for the excitation of all vibration modes (non-destructive tests). This input corresponded to 5% of the intensity of the 475-yrp earthquake. The frequencies and equivalent viscous damping ratios were obtained applying an identification method to the experimental response of both the bare and infilled frames. Unfortunately, it was impossible to carry out the identification of the infilled frame's frequencies after the PsD tests. Results are thus available for the original structure only (uncracked stiffness). On the other hand, the natural frequencies of the original bare frame were also assessed through modal dynamic tests carried out with an instrumented (load cell) impact hammer of 5 kg mass, which allowed for the validation of the results obtained with the non-destructive tests.

The bare frame (BF) performed satisfactorily during the 475-yrp earthquake test, showing only minor local damage without significant consequences. On the other hand, it sustained extensive damage at the third storey level during the 975-yrp earthquake test, which had to be stopped at half-time due to its imminent collapse (as such, there was no reason to perform the 2000-yrp earthquake test). The above-referred numerical models developed by Falcão Moreira [10] were able to significantly reproduce this behaviour, including the sudden formation of the soft-storey mechanism at the third storey. Hinging developed at the top, bottom, and rebar lap-splice (70 cm from bottom) sections of the strong column, causing the third storey to experience severe deformation. However, only concrete cover spalling and the yielding of rebars took place. Neither buckling nor rupture occurred. In addition, no stirrups disclosure or rupture occurred, except at the lap-splice zone. The sudden reduction of the cross-section's height and reinforcement ratio (plus the consequent lap-splice) contributed to the concentration of damage at this location. Figure 11 shows the observed damage pattern.



(...) Crack opening (mm)

Figure 11. Damage pattern after the BF tests (adapted from [29]).

Regarding the performance of the infilled frame (IN), the latter was subjected to the three consecutive earthquake signals (475-, 975-, and 2000-yrp). During the 475-yrp test, it behaved quite well. Minor cracking was observed only around the infill openings at the first and second storeys, as well as separation between the infill panels and the surrounding RC members. No significant cracking was observed in any of the RC members. The 975-yrp test, on the other hand, caused a significant amount of damage to the bottom storey's infills (shear cracking became significant), along with some minor damage to the RC beam-column joints and several columns at this level. Smaller amounts of damage in similar locations were noted in the second storey, while no significant damage was observed in the upper two storeys. In summary, at the end of this test, the RC structure was found to be in good condition at all levels, as were the infills at the second, third, and fourth storeys. However, the first storey infills were severely damaged (too damaged even to be retrofitted). Given this situation (i.e., the imminent formation of a soft-storey mechanism at the first storey), the 2000-yrp test was run for only 5 s in order to study how gradually the lateral strength dropped off with increasing drift. The damage patterns at the end of this test were essentially more severe versions of what had been observed during the 975-yrp test. What remained from the first storey infills was severely damaged, with the formation of wide diagonal cracks on all three panels. Significant shear cracks (approx. 4 mm wide) developed at the bottom section of the strong column along with the spalling of the concrete cover. However, the previous cracking patterns on the other RC members showed no significant change. Very little new damage occurred in the upper storeys. The overall structural behaviour was clearly that of a soft-storey structure. Figure 12 shows the observed damage pattern.

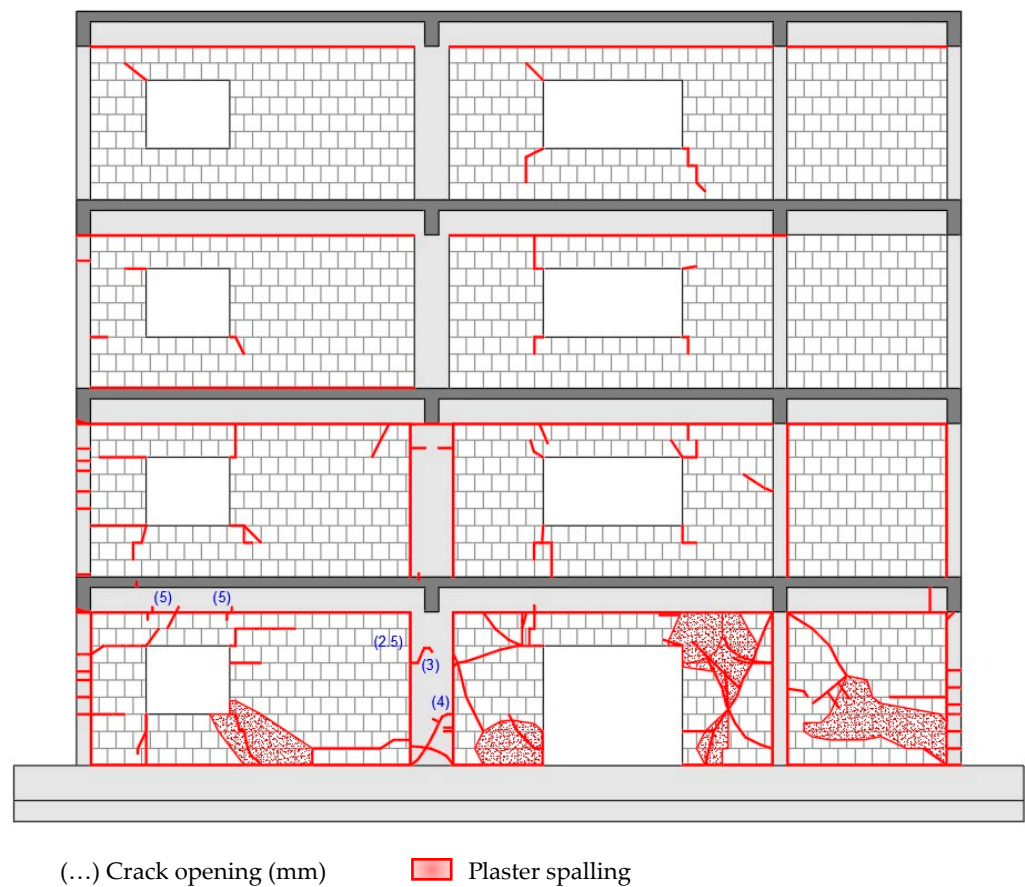


Figure 12. Damage pattern after the IN tests (adapted from [29]).

The results of the tests performed on the BF confirmed the soft-storey mechanism which was expected to develop due to the vertical irregularity induced by the sudden reduction in the strong column's cross-section. This structural misconception is common in older-type RC buildings and a frequent collapse inducer during earthquake response. In this case, despite the very limited damage observed after the 475-yrp earthquake test, the demands for a slightly more intense earthquake (1.3 times the maximum acceleration of the 475-yrp record) led to imminent storey failure and the consequent collapse of the structure. This is consistent with the high vulnerability which is typical of such structures. Concerning the effect of the masonry infill walls on the seismic response, conclusions are clear when comparing the results of the bare and infilled tests. The infill panels substantially increased the initial stiffness and strength at the storey level and, consequently, the global stiffness and strength of the structure. The maximum strength reached for the first storey of the infilled frame was about four times the value for the bare structure. However, the brittleness of the infilled structure after reaching its maximum strength was noticeable (i.e., the rapid decrease of the first storey's strength). Significant changes were also observed in terms of inter-storey drift profiles. The concentration of damage at the third storey of the irregular RC frame did not occur during the IN tests (in fact, the infill panels prevented the development of an irregular structural response). The above-referenced numerical models developed by Falcão Moreira [10] were also able to reproduce this behaviour. For further details, readers are referred to [9,10,29].

3.3. Numerical Modelling

The *SeismoStruct* software platform [30] was used to develop nonlinear analysis models for both the bare and infilled frames. Figure 13 displays the general characteristics of the BF model. The RC frame members were modelled using a distributed plasticity model with approximately 200 fibres per cross-section. A force-based FE formulation was

implemented, with one FE per member and five integration sections per element, following the recommendations of Calabrese et al. [31]. The cyclic behaviour of the concrete and steel rebar materials were respectively defined using the Mander et al. model [32] and the Menegotto and Pinto model [33], combined with isotropic hardening rules proposed by Filippou et al. [34]. The mechanical properties of the materials used were as follows (mean values): concrete compressive strength $f_c = 11.98$ MPa; concrete tensile strength $f_t = 1.20$ MPa; concrete modulus of elasticity (initial elastic stiffness) $E_c = 21.65$ GPa; concrete strain at unconfined peak compressive stress $\epsilon_c = 0.0025$ m/m; concrete specific weight $\gamma_c = 2450$ kg/m³; steel yield stress $f_y = 343.60$ MPa; steel modulus of elasticity (initial elastic stiffness) $E_s = 204.50$ GPa; steel strain hardening parameter $\mu = 0.0024$; and steel specific weight $\gamma_s = 7850$ kg/m³. Further details can be found in [10].

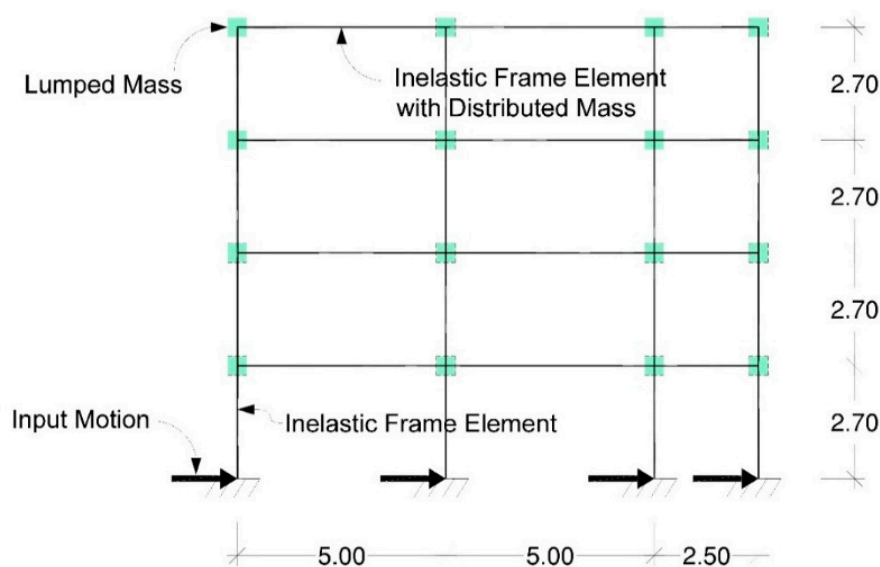


Figure 13. General characteristics of the numerical model developed for the BF.

The nonlinear cyclic model for masonry panels developed by Crisafulli [19]—briefly presented in Section 2 and implemented in *SeismoStruct* by Blandon [35]—was used to model the infill walls. As previously mentioned, this model has the advantage of accounting for the local effects caused by the infill panels in the surrounding frame without a significant increase in the complexity of the analysis. However, it does require the definition of a large number of parameters to fully characterize the nonlinear element. These parameters may be organized in three groups according to their nature: (i) mechanical; (ii) geometrical; and (iii) empirical. The mechanical and geometrical parameters define the monotonic behaviour of the strut elements, while the empirical parameters are exclusively associated with the cyclic loading rules. The adopted final values (presented below) were set according to available experimental results and/or the recommendations of Crisafulli [19], Smyrou et al. [11], and O'Reilly [12].

Due to their different characteristics, the infill panels were divided into four groups with specific parameters: (i) “Full_IN”, including all the short panels with no openings; (ii) “Door_IN”, including the central long panel with a door opening at the 1st storey; (iii) “LargeW_IN”, including the central long panels with large window openings at the second, third, and fourth storeys; and (iv) “SmallW_IN”, including all the external long panels with small window openings. Table 1 summarizes the general dimensions of each panel group, where L is the span of beam between centre line of supporting columns; H is the storey height; l_w is the length of the masonry panel between adjacent columns; h_w is the height of the masonry panel; t_w is the thickness of the masonry infill (12 cm thick bricks + 1.5 cm of plaster on each side); b and d are, respectively, the height and length of the bricks; d_w is the diagonal length of the masonry panel; and θ is the inclination of the

diagonal of the masonry panel to the horizontal axis. The size of the openings are given as width \times height.

Table 1. Dimensions of masonry infill walls according to the defined groups (see Figure 10).

	Full_IN	Door_IN	LargeW_IN	SmallW_IN
L (m)	2.50	5.00	5.00	5.00
H (m)	2.70	2.70	2.70	2.70
l_w (m)	2.30	4.60	4.60	4.60
h_w (m)	2.20	2.20	2.20	2.20
t_w (m)	0.15	0.15	0.15	0.15
b (m)	0.245	0.245	0.245	0.245
d (m)	0.245	0.245	0.245	0.245
d_w (m)	3.18	5.10	5.10	5.10
θ ($^\circ$)	43.73	25.56	25.56	25.56
θ (rad)	0.76318	0.44611	0.44611	0.44611
Openings (m ²)	-	2.00 \times 1.75	2.00 \times 1.00	1.20 \times 1.00

The compression/tension cyclic relationship is characterized by six mechanical parameters: (i) initial elastic modulus E_{m0} ; (ii) compressive strength for angle θ , $f_{m\theta}$; (iii) tensile strength f_t ; (iv) strain at maximum stress ε_m ; (v) ultimate strain ε_u ; and (vi) closing strain ε_{cl} . When no sufficient experimental information exists, the usual approach is to estimate values by applying the empirical expressions and value ranges found in the literature. Along with the experimental test results, the following were used to evaluate the initial elastic modulus E_{m0} :

Refs. [36,37]

$$E_m = 750 \cdot f_m \quad (3)$$

Ref. [38]

$$E_m = 1180 \cdot f_m^{0.83} \quad (4)$$

Ref. [39]

$$E_m = 2116 \cdot \sqrt{f_m} \quad (5)$$

Refs. [36,37]

$$E_m = 1000 \cdot f_m \quad (6)$$

where f_m represents the standard compressive strength of masonry (measured in a vertical compression test) in MPa. It is worth noting, however, that these expressions define a secant modulus E_m at a stress level between one-third to two-thirds of the maximum compressive stress, while the initial elastic modulus E_{m0} represents the initial slope of the stress-strain curve. Therefore, the direct use of such values may underestimate the initial stiffness of the infilled frame. Crisafulli [19] thus recommends, in order to obtain an adequate ascending branch of the strength envelope, that $E_{m0} \geq 2 \cdot f_{m\theta} / \varepsilon_m$. These considerations led to a uniform value of $E_{m0} = 2.20$ GPa, which was used for the four infill panel groups.

The compressive strength for angle θ , $f_{m\theta}$, is the main parameter to control the resistance of the struts. It does not, however, represent the above referred standard compressive strength of masonry, as it depends on the expected failure mode for the panel. Four basic failure modes are considered, each with a corresponding equivalent failure compressive stress: (i) diagonal tension; (ii) sliding shear along horizontal joints (the most common); (iii) crushing of corners in contact with the RC frame; and (iv) diagonal compression at the

centre of the panel. The expressions described in Decanini et al. [25–27] and O’Reilly [12] for each failure mode are given below in the same order:

$$\sigma_{w,DT} = \frac{0.6 \cdot f_{ms} + 0.3 \cdot \sigma_v}{\frac{b_w}{d_w}} \quad (7)$$

$$\sigma_{w,SH} = \frac{(1.2 \cdot \sin \theta + 0.45 \cdot \cos \theta) \cdot f_{mu} + 0.3 \cdot \sigma_v}{\frac{b_w}{d_w}} \quad (8)$$

$$\sigma_{w,CRN} = \frac{1.12 \cdot \sin \theta \cdot \cos \theta}{K_1 \cdot (\lambda H)^{-0.12} + K_2 \cdot (\lambda H)^{0.88}} \cdot f_m \quad (9)$$

$$\sigma_{w,DC} = \frac{1.16 \cdot \tan \theta}{K_1 + K_2 \cdot \lambda H} \cdot f_m \quad (10)$$

where f_{ms} is the shear strength measured in diagonal compression tests; σ_v is the vertical compression stress due to gravity loads (usually equal to zero, as infill panels are typically not load-bearing); b_w is the equivalent width of the strut; f_{mu} is the sliding resistance of mortar joints measured in triplet tests; λH is a non-dimensional parameter—originally proposed by Stafford Smith [24] and given below by Expression (11)—which expresses the relative stiffness of the infill panel to the RC frame; K_1 and K_2 are two constants which depend on the value of λH and on the cracking state of the infill panel (i.e., cracked or uncracked), and are also given below.

$$\lambda H = H \cdot \sqrt[4]{\frac{E_m \cdot t_w \cdot \sin 2\theta}{4 \cdot E_c \cdot I_c \cdot h_w}} \quad (11)$$

Cracked panel:

$$\begin{aligned} \lambda H < 3.14 &\Rightarrow K_1 = 1.300; K_2 = -0.178 \\ 3.14 \leq \lambda H \leq 7.85 &\Rightarrow K_1 = 0.707; K_2 = 0.010 \\ \lambda H > 7.85 &\Rightarrow K_1 = 0.470; K_2 = 0.040 \end{aligned} \quad (12)$$

Uncracked panel:

$$\begin{aligned} \lambda H < 3.14 &\Rightarrow K_1 = 1.375; K_2 = -0.115 \\ 3.14 \leq \lambda H \leq 7.85 &\Rightarrow K_1 = 0.748; K_2 = 0.085 \\ \lambda H > 7.85 &\Rightarrow K_1 = 0.393; K_2 = 0.130 \end{aligned} \quad (13)$$

In Expression (11), E_c and I_c represent the elastic modulus of concrete and the moment of inertia of the adjacent columns, respectively. It should be kept in mind, however, that the value of I_c significantly decreases after cracking develops in the columns. The value of E_m to be used should also correspond to the considered state of the infill panel (cracked or uncracked). Concerning coefficients K_1 and K_2 , these were initially introduced by Decanini and Fantin [40], and were later adapted by Bertoldi et al. [41]. However, as values for when $\lambda H < 3.14$ in an uncracked panel state are not found in these references, those shown in Expression (13) are proposed herein by the authors. Given all these considerations, the equivalent failure compressive stresses corresponding to each failure mode can be determined, with the most likely to occur being defined by the minimum value. The latter should then be taken equal to the panel’s $f_{m\theta}$. This process led to values of 1.00 MPa and 0.50 MPa for the short (Full_IN) and long (Door_IN, LargeW_IN and SmallW_IN) panels, respectively.

The tensile strength f_t represents either the fundamental tensile strength of masonry, or the bond strength of the panel-frame interfaces (whichever is smaller). Its consideration brings generality to the model; however, as it has no significant influence on the overall response, it can be assumed as equal to zero in the absence of better information. The strain

at maximum stress ε_m influences the overall response of the infilled frame through the modification of the secant stiffness of the ascending branch of the stress-strain curve. This parameter usually varies between -0.001 and -0.005 , but should be calibrated based on experimental data. The ultimate strain ε_u is a parameter used to control the descending branch of the stress-strain relationship. The adoption of a large value such as $\varepsilon_u = 20 \cdot \varepsilon_m$ ensures a smooth decrease of the strut's compressive stress. Lastly, the closing strain ε_{cl} defines the limit strain at which cracks partially close and compressive stresses can develop. Values ranging between 0 and 0.003 lead to results which are in sufficient agreement with the experimental data. Alternatively, if a large negative value is adopted (e.g., $\varepsilon_{cl} = \varepsilon_u$), this effect is not considered in the analysis. Table 2 shows the final values adopted for these parameters.

Table 2. Final limit strains for the calibration of the compression/tension cyclic relationship.

	Full_IN	Door_IN	LargeW_IN	SmallW_IN
ε_m	-0.0010	-0.0008	-0.0008	-0.0008
ε_u	-0.0200	-0.0160	-0.0160	-0.0160
ε_{cl}	0.0030	0.0030	0.0030	0.0030

In addition to the above-described mechanical parameters, a set of nine empirical (less intuitive and harder to calibrate) factors is required to complete the characterization of the compression/tension cyclic relationship:

- Unloading stiffness factor (γ_{un}): this defines the unloading modulus in proportion to E_{m0} , thus controlling the slope of the unloading branch, modifying the internal cycles but not the envelope;
- Reloading strain factor (α_{re}): this predicts the strain at which the reloading curve reaches the strength envelope;
- Inflection strain factor (α_{ch}): this predicts the strain at which the reloading curve should feature an inflexion point, thus controlling the loops' "fatness";
- Unloading strain factor (β_a): this defines an auxiliary point to determine the plastic deformation after complete unloading;
- Inflection stress factor (β_{ch}): this predicts the stress at which the reloading curve should feature an inflexion point;
- Zero stress stiffness factor (γ_{plu}): this defines the modulus of the hysteretic curve at zero stress, in proportion to E_{m0} , after complete unloading has occurred;
- Reloading stiffness factor (γ_{plr}): this defines the modulus of the reloading curve, in proportion to E_{m0} , after complete unloading has occurred;
- Plastic unloading stiffness factor (e_{x1}): this defines the unloading tangent modulus corresponding to the plastic strain in proportion to E_{m0} ;
- Repeated cycle strain factor (e_{x2}): this defines the strain that the envelope curve should reach after inner cycling, thus representing the cumulative damage inside the repeated cycles.

Crisafulli [19] defined the limits for which each parameter has meaning, and proposed a range of recommended values based on experimental results. A few years later, Smyrou et al. [11] carried out a sensitivity study that seems to show that, when running nonlinear dynamic analyses, only three of these parameters (γ_{un} , α_{ch} , e_{x1}) play significant roles in the energy dissipation capacity of the infill panel (i.e., the remaining parameters are not expected to have a major impact if changed from the proposed default values). Table 3 shows the recommended range and final adopted values for these parameters (valid for the four infill panel groups).

Table 3. Empirical parameters: limits recommended by Crisafulli [19], and final adopted values.

	Recommended Range	Limits	Adopted Value
γ_{un}	1.5–2.5	≥ 1	1.70
α_{re}	0.2–0.4	≥ 0	0.20
α_{ch}	0.3–0.6	0.1–0.7	0.70
β_a	1.5–2.0	≥ 0	2.00
β_{ch}	0.6–0.7	0.5–0.9	0.90
γ_{plu}	0.5–0.7	0–1	1.00
γ_{plr}	1.1–1.5	≥ 1	1.10
e_{x1}	1.5–2.0	≥ 0	3.00
e_{x2}	1.0–1.5	≥ 0	1.00

Concerning the cyclic shear relationship, four parameters need to be defined to fully characterize this response curve: (i) initial shear bond strength τ_0 ; (ii) friction coefficient μ ; (iii) maximum permissible shear stress τ_{max} ; and (iv) shear stress distribution factor α_s . The values of τ_0 and μ can either be evaluated by direct shear tests or obtained from the design specifications. However, whilst the former may lead to an overestimation of values [42,43], the latter tend to be over-conservative, so caution is advised when selecting the approach. Crisafulli [19], for instance, within the proposed modification to the Mann and Müller's [44] theory, referred the following expressions for reducing values obtained from shear tests, where τ_0^* and μ^* are, respectively, the reduced shear bond strength and the reduced friction coefficient, and C_n is a constant that can be taken equal to 1.5 for practical application.

$$\begin{aligned}\tau_0^* &= \frac{\tau_0}{1 + \mu \cdot C_n \cdot \frac{b}{d}} \\ \mu^* &= \frac{\mu}{1 + \mu \cdot C_n \cdot \frac{b}{d}}\end{aligned}\quad (14)$$

Several researchers (e.g., [37,39]) have experimentally determined the initial shear bond strength τ_0 , suggesting either relatively narrow value ranges such as 0.3 to 0.6 MPa, or broader ones such as 0.1 to 0.7 MPa, or even 0.1 to 1.5 MPa. However, the wide variety of tested materials should be noted. Empirical expressions (dependent on various parameters) have also resulted from these and other research initiatives, but should be used with caution given the large number of involved variables. In parallel, the friction coefficient μ has been reported to vary within a range as large as 0.1 to 1.2. However, some of the proposed values are meant for design applications rather than assessment, therefore being conservatively low. Atkinson et al. [45] suggested a default range of 0.70 to 0.85 for assessment purposes. These considerations led to values of τ_0 equal to 0.25 and 0.30 MPa for the modelling of the infill panels with and without openings, respectively, and to a uniform value of μ equal to 0.70.

The maximum permissible shear stress τ_{max} represents an upper limit to the infill panels' shear strength calculation as given by the hysteresis rules proposed by Crisafulli [19]. It is based upon experimental and analytical evidence indicating that values provided by such rules become unrealistic when computing medium to high values of compressive stresses at bed joints. Values for τ_{max} can be selected from the shear failure envelope given by the above referenced modification of Mann and Müller's [44] theory, depending on the expected failure mode. However, in the absence of better information, a default range of 0.5 to 1.0 MPa can be considered. Concerning the shear stress distribution factor α_s , it is used to take into account the non-uniform distribution of shear stresses along the horizontal section of the infill panels, being defined as the ratio between the maximum and average shear stresses. It usually varies between 1.40 and 1.65, with a proposed default value of 1.50, which will work well for most situations. Values of τ_{max} equal to 0.6 and 1.0 MPa

were used in this study for the modelling of the infill panels with and without openings, respectively, along with a uniform value of α_s equal to 1.50.

Finally, for the characterization of the nonlinear element to be complete, the following parameters are still required: (i) initial strut area A_1 ; (ii) residual strut area A_2 ; (iii) strut area reduction strain ε_1 ; (iv) residual strut area strain ε_2 ; (v) equivalent contact length h_z ; (vi) horizontal offset X_{oi} ; (vii) vertical offset Y_{oi} ; and (viii) shear stiffness factor γ_s . The initial strut area A_1 is defined as the product of the infill panel's thickness t_w by the equivalent width of the strut b_w , the latter typically varying between 10% and 40% of the diagonal length of the panel d_w , as reported by several authors based on experimental data. Numerous empirical expressions have also been proposed—featuring varying degrees of complexity—that can be used to estimate the value of b_w when no sufficient experimental information exists. Expressions (15) to (19) below are some of the most popular.

Ref. [46]

$$b_w = \frac{d_w}{3} \quad (15)$$

Ref. [37]

$$b_w = 0.25 \cdot d_w \quad (16)$$

Ref. [47]

$$b_w = 0.16 \cdot (\lambda H)^{-0.3} \cdot d_w \quad (17)$$

Ref. [48]

$$b_w = \frac{0.95 \cdot h_w \cdot \cos \theta}{\sqrt{\lambda H}} \quad (18)$$

Ref. [40]

$$b_w = \left(\frac{K_1}{\lambda H} + K_2 \right) \cdot d_w \quad (19)$$

From the above reference, Expression (19) has the interesting feature of being linked to Expressions (11) to (13), thus allowing for the calculation of b_w associated with both the cracked and uncracked states of the infill panel. It should be noted, however, that the values provided by these expressions refer to fully infilled panels. If openings exist in a panel, Smyrou et al. [11] suggests reducing the initial strut area A_1 in proportion to the area of the opening in relation to that of the panel, so as to consider the expected reduction of the panel's stiffness. In practical terms, this is done by reducing the value of b_w corresponding to the fully infilled panel. The value of the reduction factor will depend on the relative size of the opening to that of the panel, as already stated, but also on its location within (e.g., centred vs. near loaded ends of the compressed struts). Engineering judgement and experience are, therefore, of the utmost importance to deal with this matter for which uncertainties are still so predominant.

The residual strut area A_2 is a parameter that accounts for the fact that, due to cracking, the contact length between the frame and the infill panel decreases as the lateral and (consequently) axial displacements increase, thus affecting the area of the equivalent strut. A linear variation as a function of the axial strain is assumed between A_1 and A_2 (Figure 14). According to the experimental results reported by Decanini and Fantin [40], cracking induces a decrease of about 20% to 50% of the equivalent width of the strut. Therefore, a default range of about 50% to 80% can be used to define A_2 as a percentage of A_1 absent better information. Concerning the definition of the strut area reduction strain ε_1 and the residual strut area strain ε_2 , these are parameters for which it is (obviously) difficult to find experimental evidence. Crisafulli [19] suggests using estimated values of $\varepsilon_m/10$ and $\varepsilon_m/2$, respectively, if no better information is available. Other authors have proposed default value ranges that can also help to determine the starting values for these parameters.

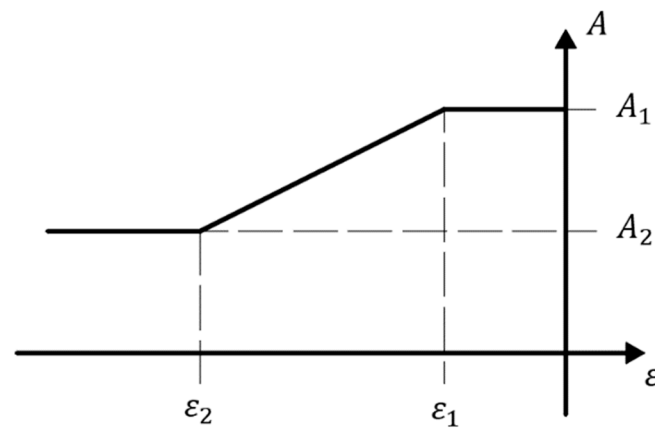


Figure 14. Equivalent strut area variation as a function of the axial strain.

The equivalent contact length h_z represents the vertical distance between the compression/tension struts, thus accounting for the actual contact length z between the frame and the infill panel, as defined by Expression (20), as proposed by Stafford Smith [24]. In Crisafulli's [19] model, given that it is a double-strut model, h_z is typically taken as equal to $z/3$ and introduced as a percentage of the storey's height, H . The geometrical definition of the contact length z is shown in Figure 15, along with that of several other geometrical parameters that have been referenced up to this point. Concerning the horizontal and vertical offsets X_{oi} and Y_{oi} , these are introduced as a percentage of the beam's centreline span L and storey height H , respectively, and represent the reduction of the latter due to the depth of the frame's members. Lastly, the shear stiffness factor γ_s represents the percentage of the total stiffness of the element to be assigned to the shear spring, thus also affecting the stiffness of the compression/tension struts. A default range of 50% to 75% is suggested by Crisafulli et al. [13], to be used given the lack of better information.

Ref. [24]

$$z = \frac{\pi}{2 \cdot \lambda H} \cdot H \quad (20)$$

Ref. [19]

$$h_z = \frac{z}{3} \quad (21)$$

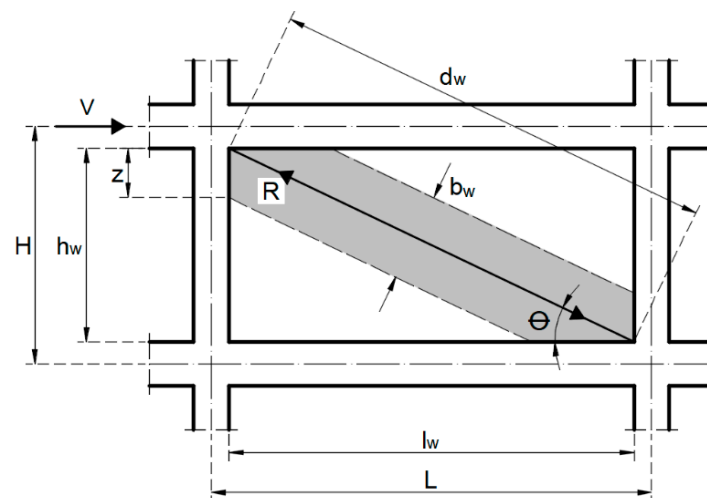


Figure 15. Geometrical properties of the infill panel and surrounding RC frame.

Table 4 shows the final values adopted herein for the above referred parameters (after several iterations of comparing numerical and experimental results). The values of b_w were estimated with the help of Expressions (15)–(19), thus referring to the equivalent width

of the strut of the fully infilled panels (i.e., with no reduction due to the openings). The reduction factors r_{ac} —defining the ratio of the strut areas A_1 of the panels with openings to that of the fully infilled panels—were obtained following the above-mentioned recommendations of Smyrou et al. [11], combined with the information provided by the available experimental results in terms of the strength and stiffness of the individual panels. It is worth noting that the values of the equivalent contact length h_z —obtained with Expressions (11), (20) and (21)—were also corrected as to somehow consider the effect of the reduction factors r_{ac} on the equivalent width of the struts b_w . Even though no evidence of this procedure was found in the reviewed literature, it made sense to the authors and the agreement between numerical and experimental results seemed to be well influenced by it. Concerning the remaining parameters, all were calibrated based on the information provided by the available experimental results, except the horizontal and vertical offsets X_{oi} and Y_{oi} that only depend on the geometry of the panel vs. that of the RC frame elements.

Table 4. Geometrical parameters: final adopted values.

	Full_IN	Door_IN	LargeW_IN	SmallW_IN
b_w (m)	1.10	2.60	2.60	2.60
b_w/d_w	0.35	0.51	0.51	0.51
r_{ac} (% b_w)	100%	18%	26%	35%
A_1 (m^2)	0.1650	0.0690	0.1006	0.1381
A_2 (% A_1)	70%	50%	50%	60%
ε_1	−0.0005	−0.0001	−0.0001	−0.0002
ε_2	−0.0008	−0.0003	−0.0003	−0.0004
h_z (% H)	9.40%	3.15%	4.59%	6.30%
X_{oi} (% L)	4.00%	6.00%	6.00%	6.00%
Y_{oi} (% H)	9.26%	9.26%	9.26%	9.26%
γ_s	70%	40%	40%	60%

Concerning the modelling of damping effects, given that the hysteretic component is implicitly included in the nonlinear model formulation/force-deformation laws describing the post-yield behaviour of inelastic elements under cyclic loading, only the effects of other (non-modelled) energy dissipation mechanisms need to be added as viscous damping (VD). The value to be employed will depend (among other things) on the imposed deformation level; i.e., low deformation levels may justify VD values that are higher than those used in analyses during which buildings are pushed deep into their inelastic range (in the latter case, the contribution of the non-modelled energy dissipation mechanisms is likely to be even smaller). From the available options to introduce VD in nonlinear analysis models, the tangent stiffness-proportional damping (TSPD) approach was used in this study. The value of the stiffness matrix multiplier α_K was thus defined by Expression (22):

$$\alpha_K = \frac{T_1 \cdot \zeta_0}{\pi} \quad (22)$$

where T_1 is the period of the vibration mode with the highest base shear, and ζ_0 is the defined VD ratio (percentage of critical). The TSPD matrix $[C] = \alpha_K \cdot [K]$ was then automatically updated at every load increment during the analyses. The values of ζ_0 introduced in the models varied with the return period of the earthquake demand, and were different for the BF and IN. After several runs and subsequent comparisons between experimental and numerical results, the best agreement was found with the following setup: (i) 475-yrp: $\zeta_0(BF) = 1.0\%$; $\zeta_0(IN) = 0.5\%$; (ii) 975-yrp: $\zeta_0(BF) = 0.5\%$; $\zeta_0(IN) \approx 0$; (iii) 2000-yrp: $\zeta_0(IN) \approx 0$. Although some authors claim that this approach may not be totally adequate

for vibrations with amplitudes below the elastic limits, these values have been judged to reproduce reality well. It is worthy of note, however, that the IN model proved to be much more sensitive to slight variations of ξ_0 than the BF model.

3.4. Seismic Demand Definition

The base seismic demand for the EC8-3 [8] assessment process was set by the Near Collapse (NC), Significant Damage (SD, and Damage Limitation (DL) limit states' elastic response acceleration spectra corresponding to zone 1.3 of the Portuguese territory (on type B ground). The goal was to ensure coherence with the moderate-high European seismic hazard scenario represented by the input motions used in the above-described PsD tests. Figure 16 shows the comparison between the code-based spectra and the acceleration spectra of the 475- and 975-yrp input motions. Considering that the frames could be allocated to structural importance class II, EC8-3 would only require the verification of the limit state (LS) of SD. However, for this case-study's purpose, the three LS were considered. Hence, three sets of target displacements were determined for the nonlinear static analyses, while for the nonlinear dynamic analyses, seven real accelerograms were selected from a database and were scaled to define three sets of signals, each being compatible with the demand spectrum of the respective LS.

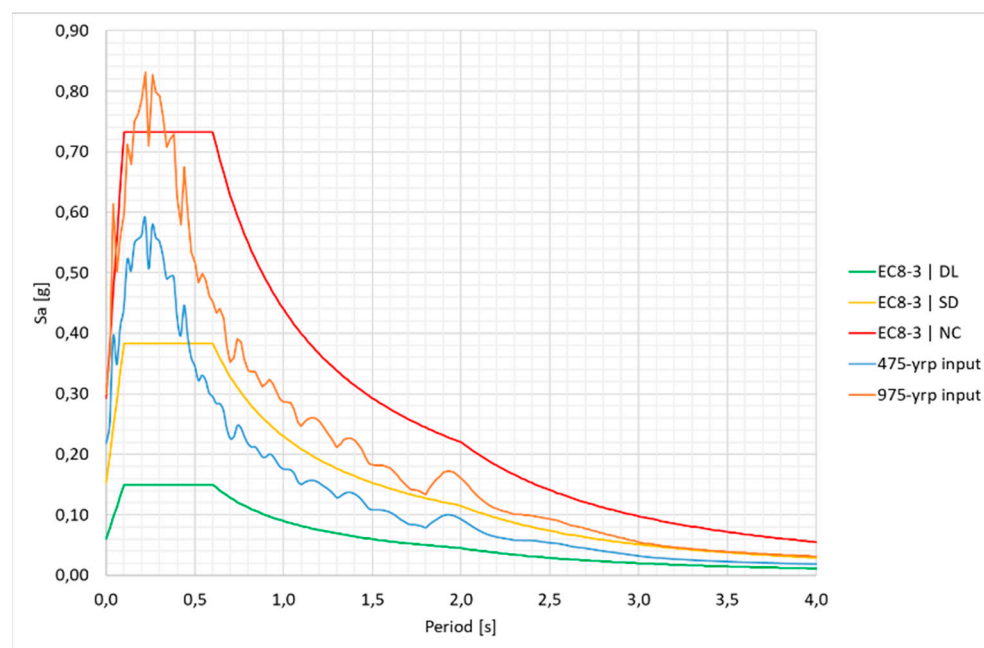


Figure 16. Comparison between the EC8-3 response acceleration spectra for seismic assessment and the elastic response acceleration spectra of the 475- and 975-yrp experimental test input motions.

The nonlinear static procedure (NSP) recommended in EC8-1 [49]—i.e., the N2 method [50]—was used to determine the target displacements for the nonlinear static analyses. As the structure lacks symmetry with regard to any axis perpendicular to the direction of the seismic action, the analysis had to be conducted for both senses of that direction (left-to-right and right-to-left). Tables 5 and 6 display the results obtained for the BF and IN, respectively, for each LS. For further information on how the target displacements were computed, readers are referred to [10].

Table 5. Target displacement values d_t for the BF (L–R: left-to-right; R–L: right-to-left).

$d_t(\text{mm})$		
LS	L–R	R–L
NC	157.1	–151.4
SD	82.0	–79.1
DL	32.1	–30.9

Table 6. Target displacement values d_t for the IN (L–R: left-to-right; R–L: right-to-left).

$d_t(\text{mm})$		
LS	L–R	R–L
NC	16.7	–16.4
SD	7.0	–6.6
DL	2.7	–2.6

The *SeIEQ* engine [51] was used to select the ground motion records for the nonlinear dynamic analyses. Seven records from actual earthquake events were chosen and were scaled to comply with both the spectral matching requirements specified in EC8-1 and the recommendations of Araújo et al. [52]. For the preliminary search conducted by *SeIEQ*, the seismological criteria were based on the features of events defining zone 1.3 in the Portuguese territory, as indicated in the country’s National Annex (NA) in EC8-1. Magnitudes and epicentral distances exceeding 5.5 and 20 km (respectively) were considered, along with an average shear wave velocity $v_{s,30}$ in the range of 360 m/s to 800 m/s (consistent with the type B ground as defined in EC8-1). The preliminary search results were subsequently restricted by ensuring the spectral compatibility between the mean spectrum of the group and the target response spectrum within the period intervals set forth in EC8-1. During the optimization process, the scaling factors were confined to the interval of 0.5 to 2.0, the mismatch between the mean spectrum of the group and the target spectrum was limited to $\pm 10\%$, and the mismatch between each individual record and the target spectrum was limited to $\pm 50\%$. This process led to the selection of the records given in Table 7, and to the scaling factors shown in the 475-yrp column. The scaling factors to then match the spectra of the LSs of DL, SD, and NC were obtained by multiplying the values in the 475-yrp column by factors of 0.30310, 0.77540, and 1.48392, respectively, which are the ratios of the constant acceleration value of each LS spectrum to that of the 475-yrp spectrum. The scaled record sets’ individual and average spectra are displayed in Figures 17–19 alongside the corresponding EC8-3 target spectra. Further information regarding the ground motion records’ selection and scaling is available in [10].

Table 7. Selected records and scaling factors for compatibility with the EC8-3 LSs.

Record	Time Step (s)	N. Steps	475-yrp	Scaling Factor		
				DL	SD	NC
R1-TaiwanSMART1(40).dat	0.010	2913	1.17310	0.35556	0.90963	1.74079
R2-Chi-ChiTaiwan.dat	0.005	18,000	1.11645	0.33839	0.86570	1.65672
R3-Northridge-01.dat	0.010	2999	1.58148	0.47934	1.22628	2.34679
R4-ChalfantValley-02.dat	0.005	7996	1.21379	0.36790	0.94118	1.80117
R5-KocaeliTurkey.dat	0.005	6000	1.67085	0.50643	1.29558	2.47941
R6-ImperialValley-06.dat	0.010	9992	0.91789	0.27821	0.71173	1.36208
R7-WhittierNarrows-01.dat	0.020	1715	1.26163	0.38240	0.97827	1.87216

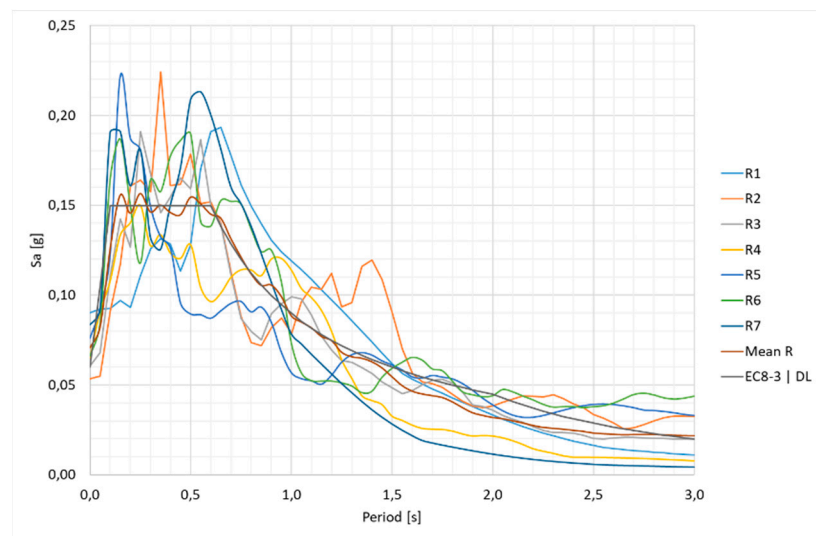


Figure 17. Ground motion records for the assessment of the EC8-3 LS of DL.

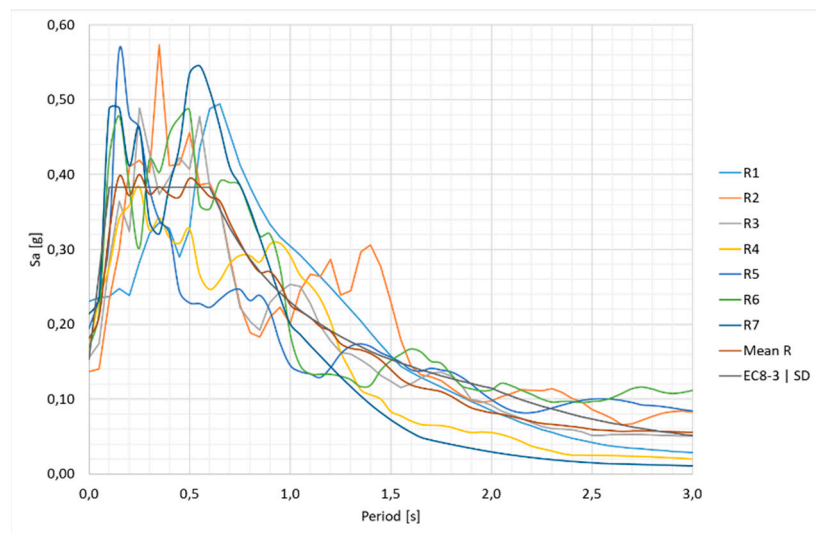


Figure 18. Ground motion records for the assessment of the EC8-3 LS of SD.

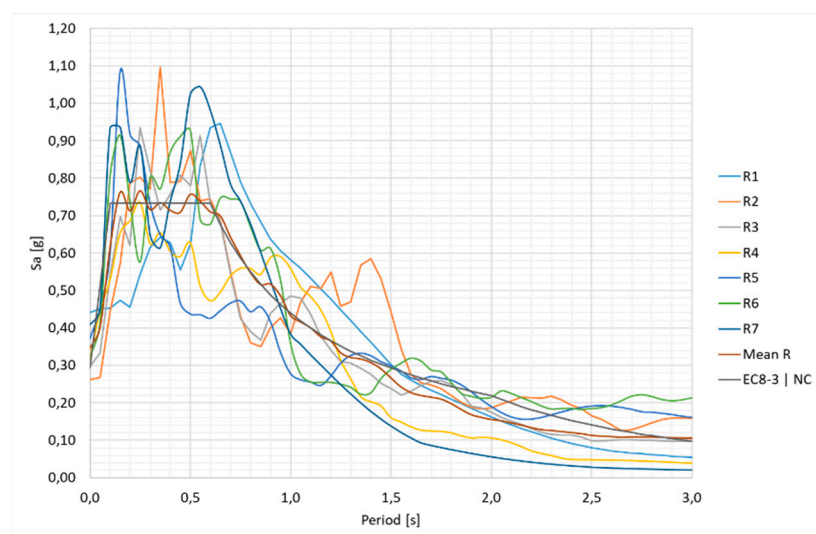


Figure 19. Ground motion records for the assessment of the EC8-3 LS of NC.

3.5. Computation of Member Capacities

The capacity values of the RC structural members were herein determined using the capacity models outlined in Annex A of EC8-3, for both deformation- and strength-controlled mechanisms (ductile and brittle, respectively). The recommendations of several authors [53–57] were followed to make the computational process less intensive and time-consuming. As the nonlinear behaviour is expected to develop at member ends, two control sections were considered within each member (the top and bottom in columns, and the left and right in beams). Figure 20 shows the numbering of the frames' members that is used henceforth. Ductile capacities were thus defined in terms of their admissible chord rotations θ for each LS, respectively θ_{NC} , θ_{SD} , and θ_{DL} . The corrective factors allowing for rebar lap-splices and/or the use of plain rebars were applied when needed (refer to clauses A.3.2.2 (3) to (5) in Annex A of EC8-3). As for brittle capacities, those were characterized by the admissible shear force V_R , subjected to the upper limits imposed by the shear capacity values obtained with the provisions of EC2-1-1. For the full details on the capacity calculation process and results, readers are referred to [10].

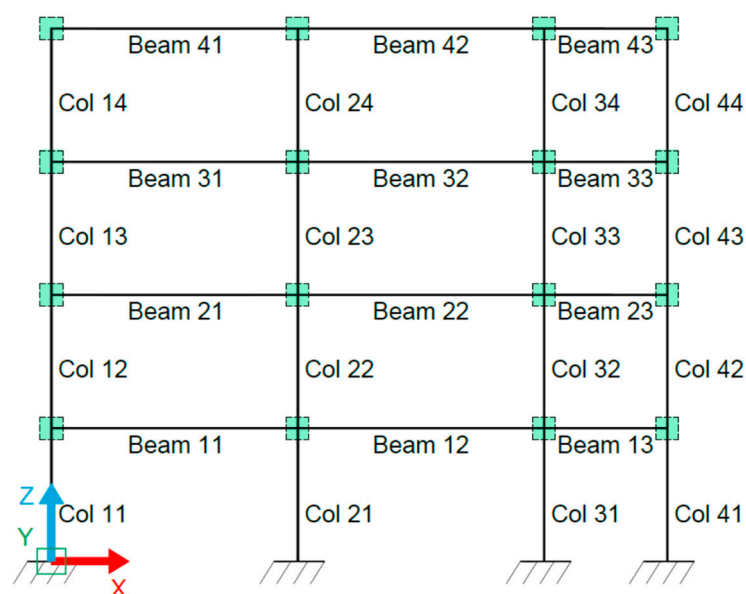


Figure 20. Numbering of the frames' RC structural members.

3.6. Performance Evaluation

Figures 21–28 display the performance evaluation results of the two analysis methods in terms of demand-to-capacity ratios (D_i/C_i) for each control section i . A ratio of 1.0 or lower indicates a safe condition, while a higher value indicates an unsafe one. For the nonlinear static (pushover) analysis models, the demand values were determined for each LS and seismic action sense at the target displacements. Therefore, the presented D/C ratios correspond to the least favourable results obtained on each control section. Conversely, the D/C ratios presented for the nonlinear dynamic analysis models are the mean values over the most unfavourable results obtained with the scaled sets of ground acceleration records. Figures 21–24 illustrate the D/C ratios (chord rotation and shear force) on the columns of the bare (BF) and infilled (IN) frames using the pushover analysis models, while Figures 25–28 depict the results obtained using the nonlinear dynamic analysis models. As for the D/C ratios for the beams, those were found to be consistently below 1.0 (which is typical of older-type RC structures with no capacity design), hence their graphical representation was intentionally excluded to save space.

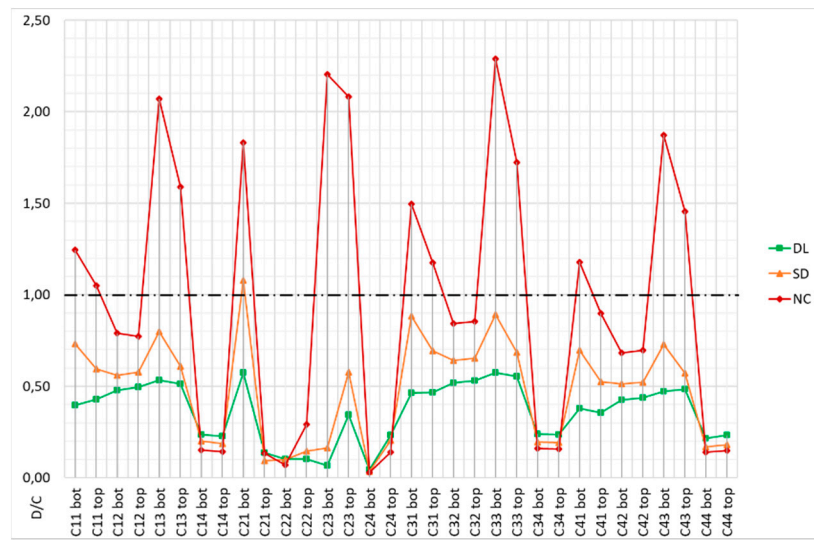


Figure 21. BF: chord rotation D/C ratios on columns (pushover analysis results).

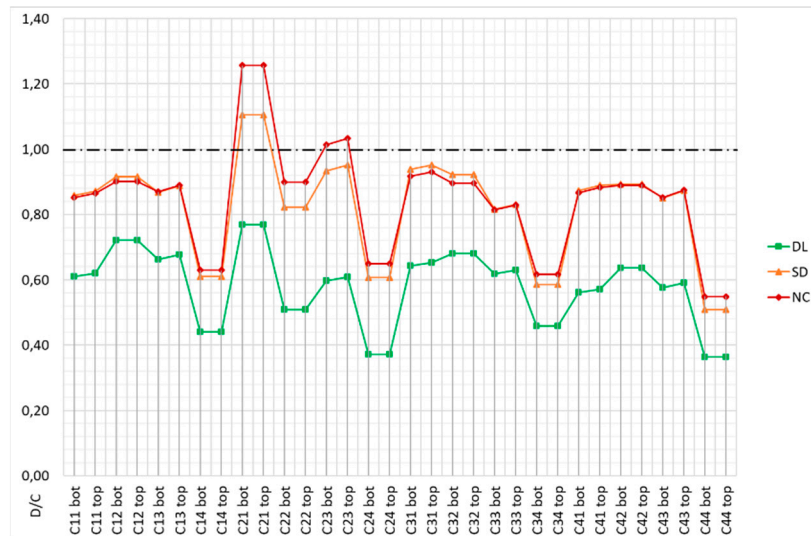


Figure 22. BF: shear force D/C ratios on columns (pushover analysis results).

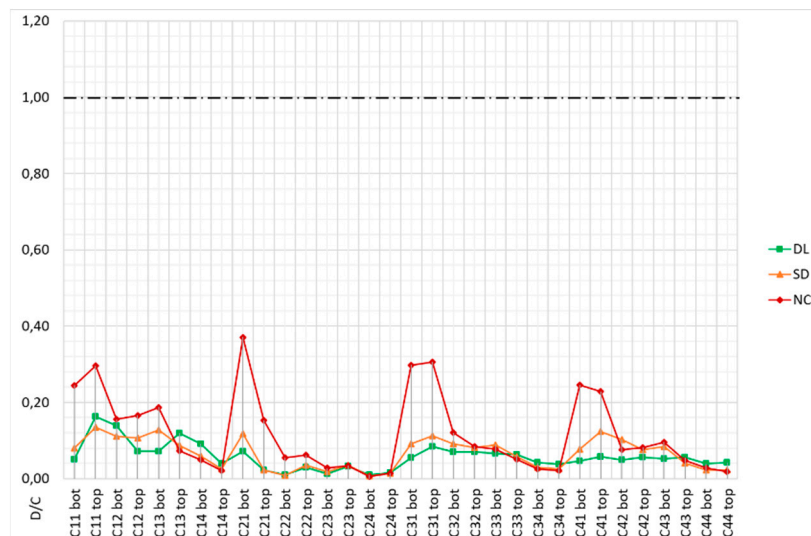


Figure 23. IN: chord rotation D/C ratios on columns (pushover analysis results).

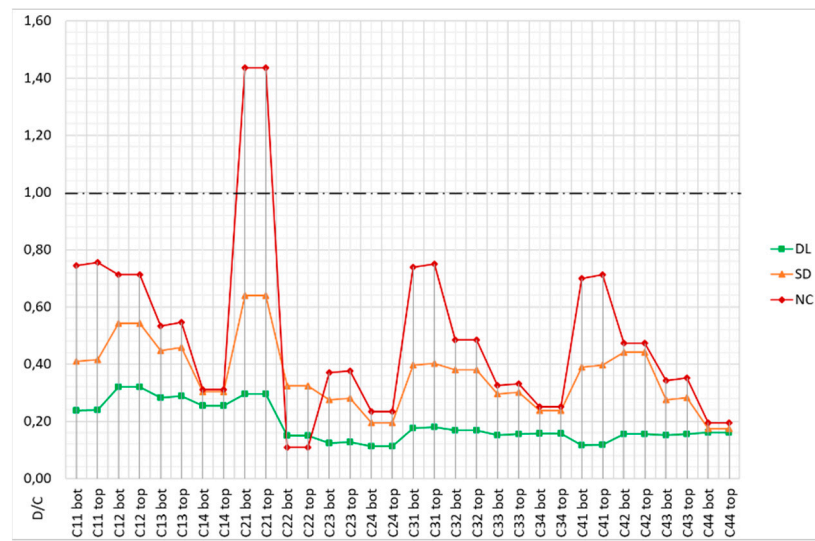


Figure 24. IN: shear force D/C ratios on columns (pushover analysis results).

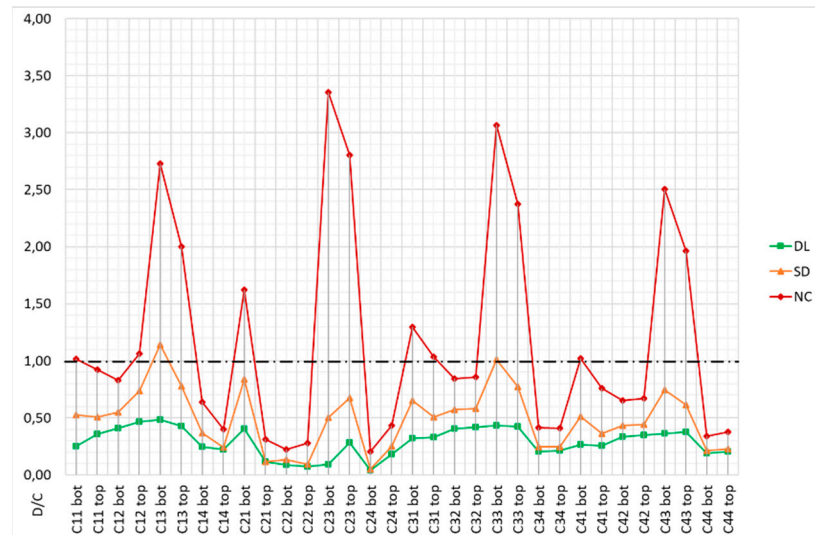


Figure 25. BF: chord rotation D/C ratios on columns (nonlinear dynamic analysis results).

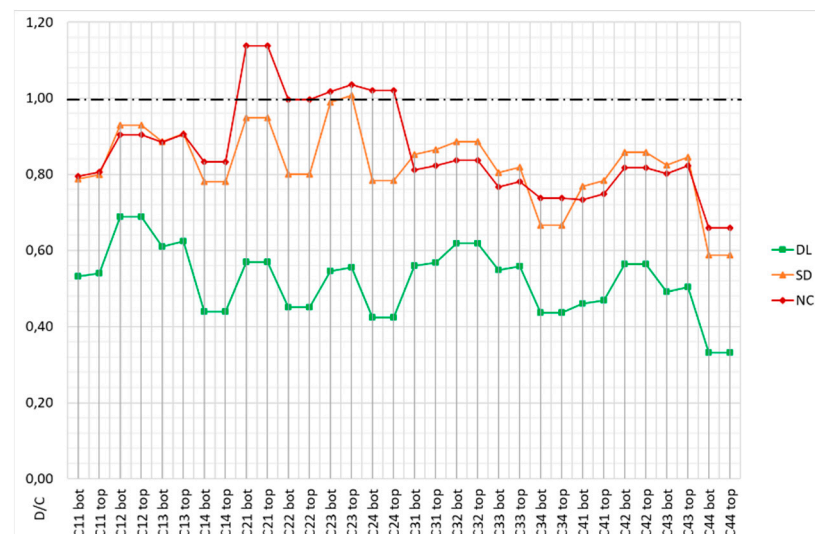


Figure 26. BF: shear force D/C ratios on columns (nonlinear dynamic analysis results).

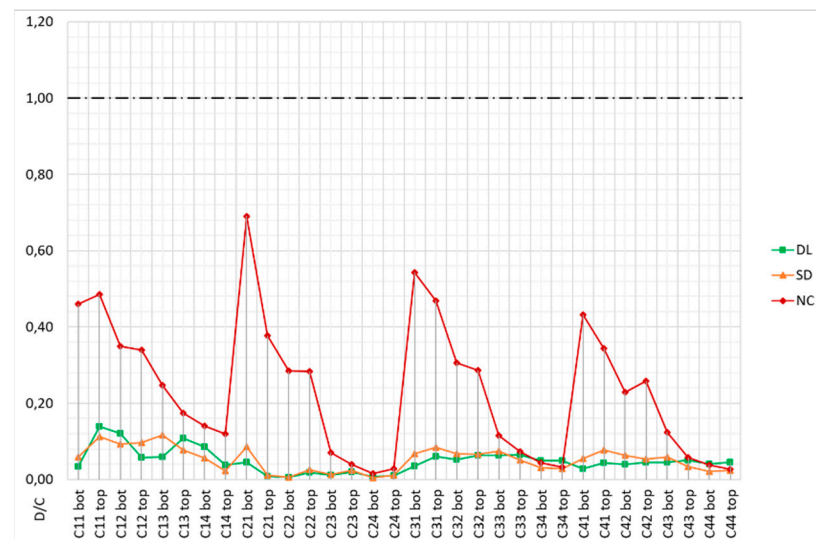


Figure 27. IN: chord rotation D/C ratios on columns (nonlinear dynamic analysis results).

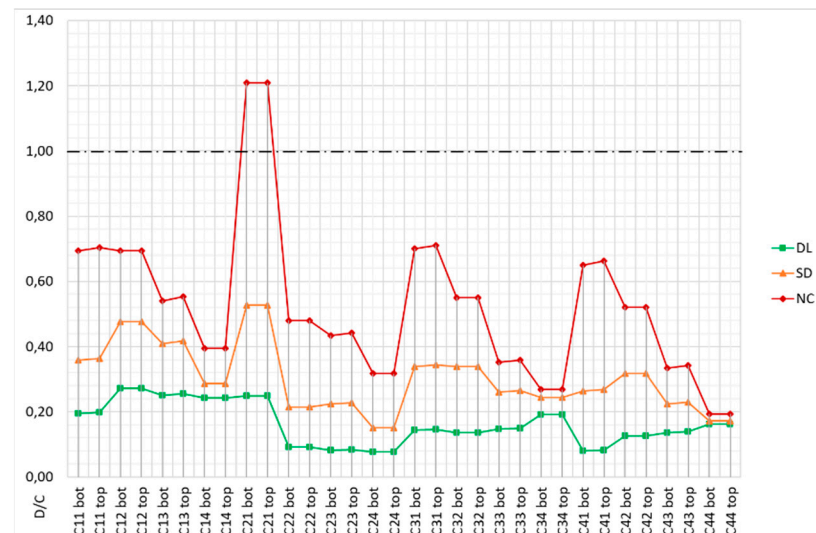


Figure 28. IN: shear force D/C ratios on columns (nonlinear dynamic analysis results).

3.7. Discussion

Before discussing the results of the seismic assessment process—and consequently drawing conclusions about the safety of the frames—it is important to compare the outcomes of the nonlinear static and dynamic analyses. Figures 21–28 (above) allow for the comparison in terms of D/C ratios, while Tables 8–10 (below) compare global storey parameters. Given the added complexity of nonlinear dynamic analysis when compared to its static equivalent, the purpose is to verify if similar conclusions are obtained, and (eventually) validate the use of pushover analysis as a swift way to evaluate the seismic performance of the frames.

Table 8. Floor displacements: nonlinear static (PSHVR) vs. dynamic (NLDA) analyses results.

Floor Displacement (mm)						
	DL		SD		NC	
BF	PSHVR	NLDA	PSHVR	NLDA	PSHVR	NLDA
Floor 4	32.1	23.6	82.0	71.8	157.1	165.4
Floor 3	27.3	20.3	73.2	62.4	148.2	151.9
Floor 2	17.0	13.2	46.0	38.0	56.7	78.1
Floor 1	6.8	5.3	20.2	16.2	26.4	40.4
	DL		SD		NC	
IN	PSHVR	NLDA	PSHVR	NLDA	PSHVR	NLDA
Floor 4	2.7	1.7	7.0	4.7	16.7	34.4
Floor 3	2.4	1.5	6.3	4.2	15.9	33.2
Floor 2	1.8	1.2	4.7	3.2	13.9	31.5
Floor 1	0.9	0.6	2.5	1.8	10.6	19.2

Table 9. Inter-storey drifts: nonlinear static (PSHVR) vs. dynamic (NLDA) analyses results.

Inter-Storey Drift (%)						
	DL		SD		NC	
BF	PSHVR	NLDA	PSHVR	NLDA	PSHVR	NLDA
Floor 4	0.18%	0.14%	0.32%	0.41%	0.33%	0.79%
Floor 3	0.38%	0.28%	1.01%	0.94%	3.10%	3.44%
Floor 2	0.38%	0.29%	0.96%	0.81%	1.14%	1.49%
Floor 1	0.25%	0.20%	0.75%	0.60%	0.99%	1.50%
	DL		SD		NC	
IN	PSHVR	NLDA	PSHVR	NLDA	PSHVR	NLDA
Floor 4	0.01%	0.01%	0.03%	0.02%	0.03%	0.05%
Floor 3	0.02%	0.01%	0.06%	0.04%	0.07%	0.09%
Floor 2	0.03%	0.02%	0.08%	0.06%	0.12%	0.49%
Floor 1	0.03%	0.02%	0.09%	0.06%	0.39%	0.71%

Table 10. Base shear: nonlinear static (PSHVR) vs. dynamic (NLDA) analyses results.

Base Shear (kN)						
	DL		SD		NC	
	PSHVR	NLDA	PSHVR	NLDA	PSHVR	NLDA
BF	126.46	112.45	191.76	185.50	204.05	216.21
IN	316.24	209.49	706.12	529.87	834.56	754.13

In terms of D/C ratios, similar results were obtained with the two approaches, leading essentially to the same assessment conclusions (i.e., the same control sections were deemed unsafe). For the LSs of DL and SD, the pushover analysis results were found to be generally conservative. On the other hand, the NC chord rotation ratios obtained with the nonlinear dynamic analysis were found to be higher (on several control sections) than those given by the pushover analysis. A closer look revealed that this was relevant for the columns located at the storeys which are prone to form soft-storey mechanisms (i.e., the third

storey in the case of the BF, and the first storey in the case of the IN). Concerning the NC shear force ratios, no relevant differences were found. The results in terms of global storey parameters also compared well, but some differences are worth mentioning. Higher parameter values were obtained with the pushover analysis for the LSs of DL and SD, for both frames. However, for the LS of NC, the highest floor displacements and inter-storey drifts were achieved by the nonlinear dynamic analysis. Nonetheless, the formation of the above-referred soft-storey mechanisms was captured well by both analysis methods (see inter-storey drift values), which constitutes an important validation of the nonlinear static approach. Concerning the NC base shear values, again no relevant differences were found between the results provided by the two analysis methods. Based on these findings, and even though the irregular response of the frames when pushed to a state of near collapse is better captured by the nonlinear dynamic method of analysis, the nonlinear static approach is deemed accurate enough for the purpose of evaluating the seismic performance of the BF and the IN.

Concerning the outcome of the seismic assessment process itself, different conclusions were reached for the BF and for the IN, depending on the LS under evaluation. For the LS of DL, the chord rotation and shear force D/C ratios were found to be below 1.0 on all control sections, thus allowing both frames to be deemed safe. However, it is noteworthy that: (i) the chord-rotation ratios of the BF are typically under 50%, while those of the IN are below 15%; and (ii) the shear force ratios of the BF are between 40% and 70%, while those of the IN are below 30%. Next, for the LS of SD, the D/C ratios of the IN continued to be quite low (below 15% and 50% for chord rotation and shear force ratios, respectively), thus allowing it to be deemed safe. On the other hand, the D/C ratios of the BF were found to be considerably high, both in terms of chord rotation and of shear force, in several control sections (even slightly above 1.0 in three of them). Signs of excessive deformation and shear force effectively started to show for this LS, respectively, on the columns of the third storey and on the strong column (C2) at all storeys. Therefore, in strict terms, and mainly due to the potentially excessive shear forces, the BF should not be deemed safe for the LS of SD. Finally, it was for the LS of NC that the most relevant differences were found between the BF and the IN. The chord rotation ratios of the latter, although exhibiting a significant increase on the columns of the first and second storeys, continued to be below 1.0 on all control sections. However, in terms of shear force, the capacity of the strong column was clearly exceeded on the first storey. Regarding the BF, its chord rotation capacities were exceeded on a considerable number of control sections, with D/C ratios above 2.5 being found on the columns of the third storey. In terms of shear force, the capacities of the strong column were exceeded on all storeys. Therefore, even though the scenario for the BF is much worse than for the IN, both frames should be deemed unsafe for the LS of NC.

The conclusions drawn above show that the option to consider (or not) the masonry infill walls in the modelling of existing RC buildings might have a significant impact on the outcome of the EC8-3 seismic assessment process. For this particular case, recalling that structural importance class II only requires the verification of the LS of SD, it would mean the difference between deeming the structure to be perfectly safe and finding it to be borderline unsafe, both in terms of deformation- and strength-controlled collapse mechanisms. The latter conclusion would most likely lead to the decision to retrofit the building, with the associated financial investment, in order to make it code compliant. As such, when low and medium seismic input motions constitute the base demand for the assessment of older-type RC-framed buildings, the protection provided to the RC members by the confined masonry infill panels should not be neglected. Therefore, the effect of the latter should be accurately modelled and analysed if reliable (and realistic) seismic performance results wish to be obtained.

A closer look at the results obtained for the LS of NC, combined with the insight provided by the experimental tests, provides additional conclusions about the collapse mechanisms of the frames and the type of retrofitting that would be more adequate. The results obtained for the BF, concerning both D/C ratios and global storey parameters,

indicate that deformation tends to be concentrated at the third storey, resulting in the formation of a soft-storey mechanism (Figure 29). They also suggest that the strong column is most likely to suffer damage due to excessive shear force, as it absorbs the majority of the total storey shear (typically more than 70%). Additionally, the chord rotation and shear force ratios on other members are high, implying that the BF would benefit the most from a global retrofitting solution capable of reducing floor displacements, eliminating the third storey's irregular response, and increasing the columns' shear capacity. The results for the IN, on the other hand, show a scenario that is quite different. Looking exclusively to the D/C ratios, one could think that the only potentially unsafe situation would be the excessive shear force on the strong column of the first storey, and just recommend a local strengthening solution. However, the inter-storey drift results and the damage by the end of the 975-yrp experimental test show the potential that exists for a soft-storey mechanism in the case of the sudden failure of the first storey infill panels (Figure 30). Therefore, to replace those infill panels by a solution capable of maintaining the storey's deformation under control and increasing the shear capacity of the selected columns, while being less vulnerable to abrupt failure, would be a safer retrofitting option. The authors thus recommend that analysts do not become dependent on just D/C ratios, but also analyse the evolution of inelastic lateral displacement profiles.

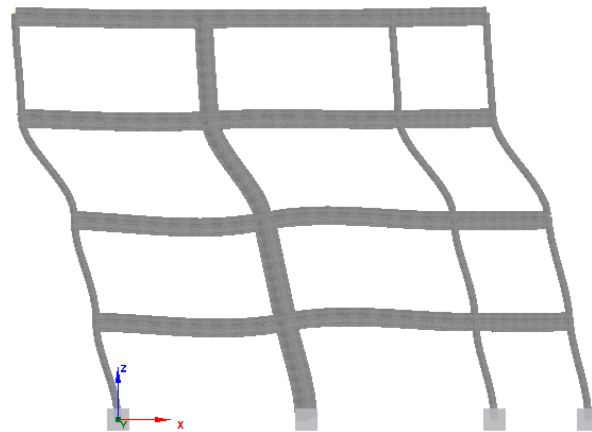


Figure 29. Soft-storey mechanism on the third storey of the BF.

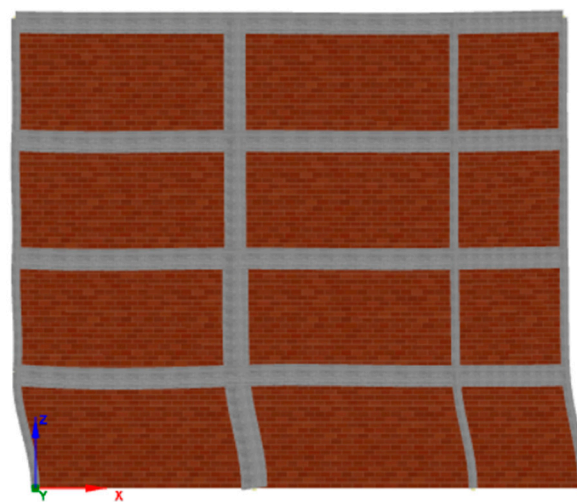


Figure 30. Soft-storey mechanism of the first storey of the IN (infill panel openings not shown).

4. Conclusions

This paper examined how the decision to include (or exclude) masonry infill walls in the modelling of non-seismically designed RC-framed structures can affect the results of the

EC8-3 seismic assessment process. A case-study application, for which experimental PsD test results are available, was presented for that purpose. Nonlinear static and dynamic analyses were carried out, and structural performance was evaluated according to the requirements of EC8-3. The coherence between numerical and experimental results was also verified. The conducted study indicates that, when low and medium seismic input motions constitute the base demand for the assessment of older-type RC framed buildings, the protection provided to the RC members by the confined masonry infill panels should not be neglected. Moreover, it showed that the identification of the most likely collapse mechanism might also suffer a significant effect from the modelling decision in question. As such, the resulting default recommendation is to include masonry infill walls in the modelling of such structures.

The discussion and conclusions extracted from this work add confidence to the EC8-3 procedure—as well as to the nonlinear static approach as a swift but reliable alternative to dynamic methods—and contribute to the calibration of nonlinear analytical models that adequately reproduce the behaviour of pre-code RC buildings. As there are still many design engineers who consider EC8-3 to be too complex to be applied in everyday practice [10], the authors hope the reported findings can help them to better understand the results provided by the seismic assessment process and thus overcome (at least) some of the experienced difficulties. However, it should be kept in mind that the modelling of infill walls is still an open issue, despite the rigorous attention it has received from the scientific community over the years [58].

Author Contributions: Conceptualization, R.F.M., H.V. and J.M.C.; Methodology, R.F.M., H.V. and J.M.C.; Formal analysis, R.F.M.; Writing—original draft preparation, R.F.M.; Writing—review and editing, R.F.M., H.V. and J.M.C. All authors have read and agreed to the published version of the manuscript.

Funding: This research was funded by: the Portuguese Foundation for Science and Technology (FCT), the individual Ph.D. grant SFRH/BD/103473/2014; “SMARTER—Seismic urban risk assessment in Iberia and Maghreb”, PT-DZ/0002/2015; “MitRisk—Framework for seismic risk reduction resorting to cost-effective retrofitting solutions”, PTDC/ECI-EST/31865/2017—POCI/01/0145/FEDER/031865, funded by FEDER funds through COMPETE2020—*Programa Operacional Competitividade e Internacionalização* (POCI), and by national funds (PIDDAC) through FCT/MCTES; Base Funding—UIDB/04708/2020 and Programmatic Funding—UIDP/04708/2020 of the CONSTRUCT—*Instituto de I&D em Estruturas e Construções*—funded by national funds through the FCT/MCTES (PIDDAC).

Data Availability Statement: The data presented in this study are available on request (please reach out to the corresponding author).

Conflicts of Interest: The authors declare that they have no conflict of interest. The funders had no role in the design of the study; in the collection, analysis, or interpretation of the data; in the writing of the manuscript; or in the decision to publish the results.

References

1. Uva, G.; Porco, F.; Fiore, A. Appraisal of masonry infill walls effect in the seismic response of RC framed buildings: A case study. *Eng. Struct.* **2012**, *34*, 514–526. [[CrossRef](#)]
2. Razzaghi, M.S.; Javidnia, M. Evaluation of the effect of infill walls on seismic performance of RC dual frames. *Int. J. Adv. Struct. Eng.* **2015**, *7*, 49–54. [[CrossRef](#)]
3. Mucedero, G.; Perrone, D.; Brunesi, E.; Monteiro, R. Numerical Modelling and Validation of the Response of Masonry Infilled RC Frames Using Experimental Testing Results. *Buildings* **2020**, *10*, 182. [[CrossRef](#)]
4. Masi, A. Seismic Vulnerability Assessment of Gravity Load Designed R/C Frames. *Bull. Earthq. Eng.* **2003**, *1*, 371–395. [[CrossRef](#)]
5. Tanganelli, M.; Viti, S.; De Stefano, M.; Rinhorn, A.M. Influence of infill panels on the seismic response of existing RC buildings: A case study. In Proceedings of the 6th European Workshop on the Seismic Behaviour of Irregular and Complex Structures, Haifa, Israel, 12–13 September 2011.
6. Kappos, A.J.; Ellul, F. Seismic design and performance assessment of masonry infilled RC frames. In Proceedings of the 12th World Conference on Seismic Engineering, Auckland, New Zealand, 30 January–4 February 2000.
7. Fajfar, P.; Dolšek, M. Seismic performance assessment of infilled reinforced concrete frames. In Proceedings of the International Conference on Earthquake Engineering and Disaster Mitigation, Jakarta, Indonesia, 25–27 September 2008.

8. EN 1998-3; Eurocode 8: Design of Structures for Earthquake Resistance—Part 3: Assessment and Retrofitting of Buildings. European Committee for Standardization: Brussels, Belgium, 2005.
9. Pinto, A.; Verzeletti, G.; Molina, J.; Varum, H.; Pinho, R.; Coelho, E. *Pseudo-Dynamic Tests on Non-Seismic Resisting RC Frames (Bare and Selective RC Frames)*; EUR Report 20244 EN. ELSA, JRC Ispra, EC, Italy; European Committee for Standardization: Brussels, Belgium, 2002.
10. Falcão Moreira, R. Seismic Risk Reduction of Reinforced Concrete Buildings Retrofitted with Steel Braces. Ph.D. Thesis, University of Porto, Porto, Portugal, 2022.
11. Smyrou, E.; Blandon, C.; Antoniou, S.; Pinho, R.; Crisafulli, F. Implementation and verification of a masonry panel model for nonlinear dynamic analysis of infilled RC frames. *Bull. Earthq. Eng.* **2011**, *9*, 1519–1534. [[CrossRef](#)]
12. O'Reilly, G.J. Performance-Based Seismic Assessment and Retrofit of Existing RC Buildings in Italy. Ph.D. Thesis, Scuola Universitaria Superiore IUSS Pavia, Pavia, Italy, 2016.
13. Crisafulli, F.J.; Carr, A.J.; Park, R. Analytical modelling of infilled frame structures—A general overview. *Bull. N. Z. Soc. Earthq. Eng.* **2000**, *33*, 30–47. [[CrossRef](#)]
14. Dias-Oliveira, J.; Rodrigues, H.; Asteris, P.G.; Varum, H. On the seismic behaviour of masonry infilled frame structures. *Buildings* **2022**, *12*, 1146. [[CrossRef](#)]
15. Kakaletsis, D.J.; Karayannis, C.G. Influence of masonry strength and openings on infilled RC frames under cyclic loading. *J. Earthq. Eng.* **2008**, *12*, 197–221. [[CrossRef](#)]
16. Messaoudi, A.; Chebili, R.; Mohamed, H.; Rodrigues, H. Influence of Masonry Infill Wall Position and Openings in the Seismic Response of Reinforced Concrete Frames. *Appl. Sci.* **2022**, *12*, 9477. [[CrossRef](#)]
17. Sassun, K.; Sullivan, T.J.; Morandi, P.; Cardone, D. Characterizing the in-plane seismic performance of infill masonry. *Bull. N. Z. Soc. Earthq. Eng.* **2015**, *49*, 100–117.
18. Furtado, A.; Rodrigues, H.; Arêde, A.; Varum, H. Simplified macro-model for infill masonry walls considering the out-of-plane behaviour. *Earthq. Eng. Struct. Dyn.* **2016**, *45*, 507–524. [[CrossRef](#)]
19. Crisafulli, F.J. Seismic Behaviour of Reinforced Concrete Structures with Masonry Infills. Ph.D. Thesis, University of Canterbury, Canterbury, New Zealand, 1997.
20. Celarec, D.; Dolšek, M. Practice-oriented probabilistic seismic performance assessment of infilled frames with consideration of shear failure of columns. *Earthq. Eng. Struct. Dyn.* **2013**, *42*, 1339–1360. [[CrossRef](#)]
21. Dolšek, M.; Fajfar, P. The effect of masonry infills on the seismic response of a four-storey reinforced concrete frame—A deterministic assessment. *Eng. Struct.* **2008**, *30*, 1991–2001. [[CrossRef](#)]
22. Jeon, J.-S.; Park, J.-H.; Des Roches, R. Seismic fragility of lightly reinforced concrete frames with masonry infills. *Earthq. Eng. Struct. Dyn.* **2015**, *44*, 1783–1803. [[CrossRef](#)]
23. Crisafulli, F.J.; Carr, A.J. Proposed macro-model for the analysis of infilled frame structures. *Bull. N. Z. Soc. Earthq. Eng.* **2007**, *40*, 69–77. [[CrossRef](#)]
24. Stafford Smith, B. Behaviour of square infilled frames. *ASCE J. Struct. Div.* **1966**, *92*, 381–403. [[CrossRef](#)]
25. Decanini, L.; De Sortis, C.A.; Goretti, A.; Langenbach, R.; Mollaioli, F.; Rasulo, A. Performance of Masonry Buildings during the 2002 Molise, Italy, Earthquake. *Earthq. Spectra* **2004**, *20*, 191–220. [[CrossRef](#)]
26. Decanini, L.D.; De Sortis, C.A.; Goretti, A.; Liberatore, L.; Mollaioli, F.; Bazzurro, P. Performance of Reinforced Concrete Buildings during the 2002 Molise, Italy, Earthquake. *Earthq. Spectra* **2004**, *20*, 221–255. [[CrossRef](#)]
27. Decanini, L.; Mollaioli, F.; Mura, A.; Saragoni, R. Seismic performance of masonry infilled RC frames. In Proceedings of the 13th World Conference on Earthquake Engineering, Vancouver, BC, Canada, 1–6 August 2004.
28. Smyrou, E. Implementation and Verification of a Masonry Panel Model for Nonlinear Dynamic Analysis of Infilled RC Frames. Master's Thesis, Università degli Studi de Pavia, Pavia, Italy, 2006.
29. Varum, H. Seismic Assessment, Strengthening and Repair of Existing Buildings. Ph.D. Thesis, University of Aveiro, Aveiro, Portugal, 2003.
30. Seismosoft (2020). SeismoStruct 2020—A Computer Program for Static and Dynamic Nonlinear Analysis of Framed Structures. Available online: <http://www.seismosoft.com> (accessed on 1 June 2020).
31. Calabrese, A.; de Almeida, J.P.; Pinho, R.J.S.M. Numerical Issues in Distributed Inelasticity Modeling of RC Frame Elements for Seismic Analysis. *J. Earthq. Eng.* **2010**, *14*, 38–68. [[CrossRef](#)]
32. Mander, J.B.; Priestley, M.J.N.; Park, R. Theoretical Stress-Strain Model for Confined Concrete. *J. Struct. Eng.* **1988**, *114*, 1804–1826. [[CrossRef](#)]
33. Menegotto, M.; Pinto, P. Method of analysis for cyclically loaded RC plane frames including changes in geometry and non-elastic behaviour of elements under combined normal force and bending. In Proceedings of the IABSE Symposium on the Resistance and Ultimate Deformability of Structures Acted on by Well Defined Repeated Loads, Zurich, Switzerland, 13–14 September 1973.
34. Filippou, F.C.; Popov, E.P.; Bertero, V.V. Modeling of R/C Joints under Cyclic Excitations. *ASCE J. Struct. Eng.* **1983**, *109*, 2666–2684. [[CrossRef](#)]
35. Blandon, C. Sensibility of nonlinear time-history analysis of a RC column using large scale shaking table results as benchmark. In Proceedings of the 15th World Conference on Earthquake Engineering, Lisbon, Portugal, 24–28 September 2012.
36. Sahlin, S. *Structural Masonry*; Prentice-Hall Inc.: Hoboken, NJ, USA, 1971; ISBN 978-0138539375.

37. Paulay, T.; Priestly, M.J.N. *Seismic Design of Reinforced Concrete and Masonry Buildings*, 1st ed.; John Wiley & Sons, Inc.: New York, NY, USA, 1992; p. 744.
38. Sinha, B.P.; Pedreschi, R. Compressive strength and some elastic properties of brickwork. *Int. J. Mason. Constr.* **1983**, *3*, 19–25.
39. Hendry, A.W. *Structural Masonry*; Macmillan Education Ltd.: London, UK, 1990; ISBN 978-1-349-14829-5.
40. Decanini, L.D.; Fantin, G.E. Modelos simplificados de la mampostería incluida en pórticos. Características de rigidez y resistencia lateral en estado límite (In Spanish). In Proceedings of the Jornadas Argentinas de Ingeniería Estructural, Buenos Aires, Argentina, 1–3 October 1986.
41. Bertoldi, S.H.; Decanini, L.D.; Gavarini, C. Telai Tamponati Soggetti ad Azione Sismica, un Modello Semplificato: Confronto Sperimentale e Numerico. In Proceedings of the Atti del 6 Convegno Nazionale ANIDIS, Perugia, Italy, 24–27 October 1993.
42. Wan, Q.; Yi, W. The shear strength of masonry walls under combined stresses. In Proceedings of the 4th Canadian Masonry Symposium, University of New Brunswick, Fredericton, NB, Canada, 2–4 June 1986.
43. Riddington, J.R.; Ghazali, M.Z. Shear strength of masonry walls. In Proceedings of the 8th International Brick and Block Masonry Conference, Dublin, Ireland, 19–21 September 1988.
44. Mann, W.; Müller, H. Failure of shear-stresses masonry—An enlarged theory, tests, and application to shear walls. *Proc. Br. Ceram. Soc.* **1982**, *30*, 139–149.
45. Atkinson, R.H.; Amadei, B.P.; Saeb, S.; Sture, S. Response of Masonry Bed Joints in Direct Shear. *ASCE J. Struct. Div.* **1989**, *115*, 2276–2296. [[CrossRef](#)]
46. Holmes, M. Steel Frames with Brickwork and Concrete Infilling. *Proc. Inst. Civ. Eng.* **1961**, *19*, 473–478. [[CrossRef](#)]
47. Mainstone, R.J. On the stiffnesses and strengths of infilled frames. *Proc. Inst. Civ. Eng.* **1971**, *49*, 57–90.
48. Liauw, T.C.; Kwan, K.H. Nonlinear behaviour of non-integral infilled frames. *Proc. Inst. Civ. Eng.* **1984**, *63 Pt 2*, 641–656.
49. *EN 1998-1*; Eurocode 8: Design of Structures for Earthquake Resistance—Part 1: General Rules, Seismic Actions, and Rules for Buildings. European Committee for Standardization: Brussels, Belgium, 2004.
50. Fajfar, P.; Fischinger, M. N2—A method for nonlinear seismic analysis of regular buildings. In Proceedings of the Ninth World Conference in Earthquake Engineering, Tokyo-Kyoto, Japan, 2–9 August 1988.
51. Macedo, L.; Castro, J. SelEQ: An advanced ground motion record selection and scaling framework. *Adv. Eng. Softw.* **2017**, *114*, 32–47. [[CrossRef](#)]
52. Araújo, M.; Macedo, L.; Marques, M.; Castro, J.M. Code-based record selection methods for seismic performance assessment of buildings. *Earthq. Eng. Struct. Dyn.* **2016**, *45*, 129–148. [[CrossRef](#)]
53. Mpampatsikos, V.; Nascimbene, R.; Petrini, L. A Critical Review of the R.C. Frame Existing Building Assessment Procedure According to Eurocode 8 and Italian Seismic Code. *J. Earthq. Eng.* **2008**, *12*, 52–82. [[CrossRef](#)]
54. Biskinis, D.E. Deformations of Concrete Members at Yielding and Ultimate. Ph.D. Thesis, University of Patra, Patra, Greece, 2006.
55. Romão, X.; Delgado, R.; Guedes, J.; Costa, A. A comparative application of different EC8-3 procedures for the seismic safety assessment of existing structures. *Bull. Earthq. Eng.* **2010**, *8*, 91–118. [[CrossRef](#)]
56. Romão, X.; Delgado, R.; Costa, A. Practical aspects of demand and capacity evaluation of RC members in the context of EC8-3. *Earthq. Eng. Struct. Dyn.* **2010**, *39*, 473–499. [[CrossRef](#)]
57. Priestley, M.J.N. *Myths and Fallacies in Earthquake Engineering, Revisited*; The Ninth Mallet Milne Lecture; IUSS Press: Pavia, Italy, 2003; ISBN 978-8873580096.
58. Asteris, P.G.; Cotsovos, D.; Chrysostomou, C.Z.; Mohebkah, A.; Al-Chaar, G.K. Mathematical micro-modelling of infilled frames: State of the art. *Eng. Struct.* **2013**, *56*, 1905–1921. [[CrossRef](#)]

Disclaimer/Publisher’s Note: The statements, opinions and data contained in all publications are solely those of the individual author(s) and contributor(s) and not of MDPI and/or the editor(s). MDPI and/or the editor(s) disclaim responsibility for any injury to people or property resulting from any ideas, methods, instructions or products referred to in the content.